Thermodynamic Casimir effect: Universality and corrections to scaling

Martin Hasenbusch*
Institut für Physik, Humboldt-Universität zu Berlin, Newtonstr. 15, 12489 Berlin, Germany
(Received 8 March 2012; published 15 May 2012)

We study the thermodynamic Casimir force for films in the three-dimensional Ising universality class with symmetry breaking boundary conditions. We focus on the effect of corrections to scaling and probe numerically the universality of our results. In particular, we check the hypothesis that corrections are well described by an effective thickness $L_{0,\mathrm{eff}} = L_0 + c(L_0 + L_s)^{1-\omega} + L_s$, where c and L_s are system specific parameters and $\omega \approx 0.8$ is the exponent of the leading bulk correction. We simulate the improved Blume-Capel model and the spin-1/2 Ising model on the simple cubic lattice. First, we analyze the behavior of various quantities at the critical point. Taking into account corrections $\propto L_0^{-\omega}$ in the case of the Ising model, we find good consistency of results obtained from these two different models. In particular, we get from the analysis of our data for the Ising model for the difference of Casimir amplitudes $\Delta_{+-} - \Delta_{++} = 3.200(5)$, which nicely compares with $\Delta_{+-} - \Delta_{++} = 3.208(5)$ obtained by studying the improved Blume-Capel model. Next, we study the behavior of the thermodynamic Casimir force for large values of the scaling variable $x = t(L_0/\xi_0)^{1/\nu}$. It can be obtained up to an overall amplitude by expressing the partition function of the film in terms of eigenvalues and eigenstates of the transfer matrix and boundary states. Here, we demonstrate how this amplitude can be computed with high accuracy. Finally, we discuss our results for the scaling functions θ_{+-} and θ_{++} of the thermodynamic Casimir force for the whole range of the scaling variable. We conclude that our numerical results are in accordance with universality. Corrections to scaling are well approximated by an effective thickness.

DOI: 10.1103/PhysRevB.85.174421 PACS number(s): 05.50.+q, 05.70.Jk, 05.10.Ln, 68.15.+e

I. INTRODUCTION

At a second-order phase transition, various quantities like the correlation length ξ or the specific heat C_{bulk} diverge following power laws such as

$$\xi \simeq \xi_{0,\pm}|t|^{-\nu}, \quad C_{\mathrm{bulk}} \simeq A_{\pm}|t|^{-\alpha}, \tag{1}$$

where $t = (T - T_c)/T_c$ is the reduced temperature, ν and α are the critical exponents of the correlation length and the specific heat, respectively. The indices $\pm$ of the amplitudes $\xi_{0,\pm}$ and $A_{\pm}$ indicate the phase: $+$ for the high temperature phase and $-$ for the low temperature phase. Critical exponents such as ν and α and amplitude ratios such as $\xi_{0,+}/\xi_{0,-}$ and A_+/A_- are universal. This means that these quantities do not depend on the microscopic details of the system but are exactly the same for all systems within a universality class. A universality class is characterized by the dimension of the system, the range of the interaction and the symmetry properties of the order parameter. For reviews on critical phenomena see, e.g., Refs. 1–4. Power laws such as Eq. (1) are valid only asymptotically in the limit $t \to 0$. At finite reduced temperature, corrections have to be taken into account:[5,6]

$$\xi = \xi_{0,\pm}|t|^{-\nu} \times (1 + a_{\pm}|t|^{\theta} + bt + c_{\pm}|t|^{2\theta} + d_{\pm}|t|^{\theta'} + \dots). \tag{2}$$

There are analytic and nonanalytic (confluent) corrections. The nonanalytic corrections are associated with nontrivial exponents $\theta = \nu\omega$, $\theta' = \nu\omega'$,.... For the universality class of the three-dimensional Ising model with short-ranged interactions, one finds consistently $\omega \approx 0.8$ from field theoretic methods, the analysis of high-temperature series expansions, and Monte Carlo simulations of lattice models.[4] Our recent estimate is $\omega = 0.832(6)$.[7] The estimate $\omega' = 1.67(11)$ obtained by the scaling field method[8] still lacks confirmation by other approaches. Furthermore, we expect corrections caused by the breaking of symmetries by the lattice. In the case of the simple cubic lattice that we consider here, these corrections are associated with $\omega'' \approx 2$.[9]

The singular behavior (1) requires that the thermodynamic limit is taken. For finite systems, the behavior of thermodynamic quantities is given by analytic functions of the parameters of the system and its linear size L_0. Finite size scaling[10] predicts that in the neighborhood of the critical point, for sufficiently large L_0, this behavior is characterized by a universal function of certain combinations of the parameters of the system and its linear size L_0. In the absence of an external field, a quantity $A(L_0,t)$ that is a function of the temperature and the linear size L_0 of the system behaves as

$$A(L_0,t) \simeq L_0^y \, g[t(L_0/\xi_{0,+})^{1/\nu}], \tag{3}$$

where the function $g(x)$ depends on the universality class of the bulk system and on the geometry of the finite system and $y = w/\nu$, where $A(\infty,t) \propto |t|^{-w}$. Also, finite size scaling is affected by corrections to scaling,[10]

$$A(L_0,t) = L_0^y \, g[t(L_0/\xi_{0,+})^{1/\nu}] \times \left\{1 + b\, q[t(L_0/\xi_{0,+})^{1/\nu}]\, L_0^{-\omega} + \dots\right\}, \tag{4}$$

where $q(x)$ is a universal function and b depends on the details of the system.

Here, we shall study films with symmetry-breaking boundary conditions. This choice is motivated by the fact that for classical binary liquid mixtures, typically, the surfaces are more attractive for one of the two components of the mixture. In addition to the corrections discussed above, these boundary conditions give rise to additional corrections where the leading one is $\propto L_0^{-1}$,[11–13] where L_0 is now the thickness of the film. In this work, we focus on the thermodynamic Casimir effect[14] in films. Due to the fact that in the neighborhood of the

critical point the range of thermal fluctuations is restricted by the finite thickness of the film, an effective force arises. The thermodynamic Casimir force per area is given by

$$F_{\rm Casimir} = -\frac{\partial \tilde{f}_{\rm ex}}{\partial L_0}, \tag{5}$$

where $\tilde{f}_{\rm ex} = \tilde{f}_{\rm film} - L_0 \tilde{f}_{\rm bulk}$ is the excess free energy per area of the film, where $\tilde{f}_{\rm film}$ is the free energy per area of the film and $\tilde{f}_{\rm bulk}$ the free energy density of the bulk system. The thermodynamic Casimir force per area follows the finite size scaling law

$$F_{\rm Casimir} \simeq k_B T L_0^{-3}\, \theta[t(L_0/\xi_{0,+})^{1/\nu}], \tag{6}$$

see, e.g., Refs. 15 and 16. For a discussion of nonuniversal contributions due to long-ranged tails of the interaction, which is not the subject of the present paper, we refer the reader to Ref. 17. After the seminal work in Ref. 14, it took about two decades until the thermodynamic Casimir effect could be demonstrated in experiments. The data obtained for films of different thicknesses of ^{4}He near the λ transition are represented to a reasonable approximation by a unique finite size scaling function.[18,19] Also experiments with liquid binary mixtures near the mixing-demixing transition were performed, where either films[20] or the sphere-plate geometry[21,22] were studied. Unfortunately, field theoretic methods do not allow to compute the scaling function $\theta(x)$ for the full range of the scaling variable.[12,13] Therefore it was an important achievement that recently the thermodynamic Casimir force was computed by Monte Carlo simulations of lattice models. Corresponding to the experiments on ^{4}He, the XY model on the simple cubic lattice was simulated.[23,24] Also the Ising model on the simple cubic lattice that shares the universality class of the mixing-demixing transition of binary mixtures was studied.[24,25] A reasonable match of the universal scaling functions θ obtained from experiments and the corresponding Monte Carlo simulations of lattice models was found. For a recent review see Ref. 26.

However, it turned out that it is quite difficult to obtain precise results for the universal scaling function θ from these Monte Carlo simulations. For the thicknesses that can be reached, corrections to scaling are still significant. Fitting the data it is difficult to disentangle corrections $\propto L^{-\omega}$ and $\propto L^{-1}$. Furthermore, the universal function $q(x)$, Eq. (4), that governs the corrections $\propto L^{-\omega}$ is *a priori* unknown. The authors of Refs. 23–25 used *ad hoc* approximations of $q(x)$ in the analysis of their data. Depending on the particular *Ansatz* that they used, the results[24,25] for the universal scaling function vary by a large amount.

In order to alleviate this problem, we studied improved models that are characterized by the fact that the amplitude of the leading bulk correction vanishes.[27,28] Since the parameter of the improved model is determined numerically, in practice, a residual amplitude remains, which is, however, at least by a factor of 30 smaller than that of the Ising and the XY models on the simple cubic lattice, respectively.[7,29] Our results for the scaling functions of the thermodynamic Casimir force agree qualitatively with those of Refs. 23–25. However, the numerical discrepancies are considerably larger than the errors that are quoted. In particular, the results obtained very recently in Ref. 30 from simulations of the Ising model by using the preferred *Ansatz* of the authors, see Eqs. (17) and (18) in Ref. 30, deviate clearly from those in Ref. 28, see Fig. 6(a) in Ref. 30, and from that in Ref. 31, see Fig. 6(b) in Ref. 30. For a discussion of this fact by the authors in Ref. 30, see the text on page 041605-9 in Ref. 30 starting about 20 lines below Table II.

The aim of the present work is to reach a better understanding of corrections to scaling. This means that we intend to determine the function $q(x)$ of Eq. (4) for the thermodynamic Casimir force. Note that due to universality of the function $q(x)$, our results might also be useful in the analysis of data obtained in experiments. Also here, we start with an *Ansatz* for $q(x)$ that is motivated as follows. The corrections $\propto L_0^{-1}$ caused by the boundaries can be expressed by a constant shift in the thickness of the film. In equations such as Eq. (3), the thickness L_0 is replaced by

$$L_{0,\rm eff} = L_0 + L_s, \tag{7}$$

where L_s depends on the details of the system but not on the observable. Here, we shall probe the hypothesis that in a similar way corrections $\propto L_0^{-\omega}$ can be taken into account by

$$L_{0,\rm eff} = L_0 + c(L_0 + L_s)^{1-\omega} + L_s. \tag{8}$$

While renormalization group arguments suggest that Eq. (7) is indeed exact, the generalization is at best a good approximation. It is motivated by the fact that for the strongly symmetry breaking boundary conditions studied here, fluctuations are suppressed in the neighborhood of the boundaries. Hence the effect of corrections to scaling should be the largest close to the boundaries. Plugging Eq. (8) into Eq. (3), ignoring the correction $\propto L_0^{-1}$ due to the boundary, we get

$$\begin{aligned} &A(L_0,t) \\ &= \left(L_0 + cL_0^{1-\omega}\right)^y\, g\left\{t\left[(L_0 + cL_0^{1-\omega})/\xi_{0,+}\right]^{1/\nu}\right\} \\ &= L_0^y\, g(x) \times \left\{1 + c\left[y + \frac{x}{\nu}\frac{g'(x)}{g(x)}\right] L_0^{-\omega} + O\left(L_0^{-2\omega}\right)\right\}, \end{aligned} \tag{9}$$

where $x = t[L_0/\xi_{0,+}]^{1/\nu}$. Hence our hypothesis (8) results in

$$q(x) = y + \frac{x}{\nu}\frac{g'(x)}{g(x)}\,. \tag{10}$$

The outline of the paper is the following. In Sec. II, we define the models that we simulated and the observables that we measured. In Sec. III, we briefly recall how finite size scaling theory applies to the free energy per area and the thermodynamic Casimir force per area. In Sec. IV, we study various quantities exactly at the critical point. Next, in Sec. V, we study the behavior of the thermodynamic Casimir force for large values of the scaling variable x. To this end, we analyze the magnetization profile near the boundary of the film and the correlation function of the bulk system. In Sec. VI, we discuss our results for the scaling functions θ_{++} and θ_{+-} in the full range of the scaling argument. Then we summarize and discuss our results. Finally, in Appendix, we discuss various results obtained for the bulk of the spin-1/2 Ising model.

II. MODEL

We study the Blume-Capel model on the simple cubic lattice. It is defined by the reduced Hamiltonian

$$H = -\beta \sum_{\langle xy \rangle} s_x s_y + D \sum_x s_x^2, \tag{11}$$

where the spin might assume the values $s_x \in \{-1,0,1\}$. $x = (x_0,x_1,x_2)$ denotes a site on the simple cubic lattice, where $x_i \in \{1,2,\ldots,L_i\}$ and $\langle xy \rangle$ denotes a pair of nearest neighbors on the lattice. The inverse temperature is denoted by $\beta = 1/k_B T$. The partition function is given by $Z = \sum_{\{s\}} \exp(-H)$, where the sum runs over all spin configurations. The parameter D controls the density of vacancies $s_x = 0$. In the limit $D \to -\infty$, vacancies are completely suppressed and hence the spin-1/2 Ising model is recovered.

In $d \geqslant 2$ dimensions, the model undergoes a continuous phase transition for $-\infty \leqslant D < D_{\rm tri}$ at a β_c that depends on D. For $D > D_{\rm tri}$, the model undergoes a first-order phase transition. Reference 32 gives for the three-dimensional simple cubic lattice, $D_{\rm tri} = 2.0313(4)$.

Numerically, using Monte Carlo simulations it has been shown that there is a point $[D^*,\beta_c(D^*)]$ on the line of second-order phase transitions, where the amplitude of leading corrections to scaling vanishes. Our recent estimate is $D^* = 0.656(20)$.[7] In Ref. 7, we simulated the model at $D = 0.655$ close to β_c on lattices of a linear size up to $L = 360$. From a standard finite size scaling analysis of phenomenological couplings like the Binder cumulant, we find $\beta_c(0.655) = 0.387721735(25)$. Furthermore, the amplitude of leading corrections to scaling is at least by a factor of 30 smaller than for the spin-1/2 Ising model. As discussed in Appendix A 1, we shall use $\beta_c = 0.22165462(2)$ as an estimate of the inverse critical temperature of the spin-1/2 Ising model in the following.

In Ref. 33, we simulated the Blume-Capel model at $D = 0.655$ in the high-temperature phase on lattices of the size L^3 with periodic boundary conditions in all directions and $L \gtrsim 10\xi$ for 201 values of β. For a few values of β, we performed new simulations that reduced the statistical error considerably. In particular, for $\beta = 0.3872$, which was our value closest to β_c, we get $\xi_{\rm 2nd}(0.3872) = 26.7013(15)$ for second moment correlation length now. Taking into account these new data, we arrive at the slightly revised result

$$\begin{aligned} \xi_{2nd,0,+} &= 0.2283(1) - 1.8(\nu - 0.63002) \\ &\quad + 275(\beta_c - 0.387721735) \\ &\text{using } t = \beta_c - \beta \text{ as definition of the reduced temperature.} \end{aligned} \tag{12}$$

The analogous result for the spin-1/2 Ising model is given in Eq. (A10) in Appendix A 2.

In the high-temperature phase, there is little difference between $\xi_{\rm 2nd}$ and the exponential correlation length $\xi_{\rm exp}$, which is defined by the asymptotic decay of the two-point correlation function. Following Ref. 34,

$$\lim_{t \searrow 0} \frac{\xi_{\rm exp}}{\xi_{\rm 2nd}} = 1.000200(3) \tag{13}$$

for the thermodynamic limit of the three-dimensional system. Note that in the following, ξ_0 always refers to $\xi_{\rm 2nd,0,+}$.

A. Film geometry and boundary conditions

In the present work, we study the thermodynamic Casimir effect for systems with film geometry. In the ideal case, this means that the system has a finite thickness L_0, while in the other two directions the thermodynamic limit $L_1,L_2 \to \infty$ is taken. In our Monte Carlo simulations, we shall study lattices with $L_0 \ll L_1,L_2$ and periodic boundary conditions in the 1 and 2 directions. Throughout, we shall simulate lattices with $L_1 = L_2 = L$.

In the 0 direction, we take symmetry breaking boundary conditions. A strong breaking of the symmetry is achieved by fixing the spins at the boundary to either -1 or 1. Here, we shall put these fixed spins on the layers at $x_0 = 0$ and at $x_0 = L_0 + 1$. This means that L_0 gives the number of layers with fluctuating spins. In the following, we shall consider the two choices: (i) $++$ boundary conditions: $s_x = 1$ for all x with $x_0 = 0$ or $x_0 = L_0 + 1$, and (ii) $+-$ boundary conditions: $s_x = 1$ for all x with $x_0 = 0$ and $s_x = -1$ for all x with $x_0 = L_0 + 1$. Note that these boundary conditions are physically relevant for experiments with confined near-critical binary mixtures, since typically a surface is more attractive to one of the components than to the other. In experiments, see, e.g., Refs. 20–22, both possible situations can be realized; both surfaces prefer the same component or one of the surfaces prefers one component, while the other surface prefers the other component of the mixture.

B. Free energy, energy and specific heat

For bulk systems, we define the reduced free energy density as

$$f_{\rm bulk} = -\frac{1}{L_0 L_1 L_2} \ln Z. \tag{14}$$

This means that compared with the free energy density $\tilde{f}_{\rm bulk}$, a factor $k_B T$ is skipped. Correspondingly, we define the energy density as the derivative of minus the reduced free energy density with respect to β:

$$E_{\rm bulk} = \frac{1}{L_0 L_1 L_2} \frac{\partial \ln Z}{\partial \beta} = \frac{1}{L_0 L_1 L_2} \left\langle \sum_{\langle x,y \rangle} s_x s_y \right\rangle, \tag{15}$$

and the specific heat

$$\begin{aligned} C_{\rm bulk} &= \frac{\partial E_{\rm bulk}}{\partial \beta} \\ &= \frac{1}{L_0 L_1 L_2} \left[\left\langle \left(\sum_{\langle x,y \rangle} s_x s_y \right)^2 \right\rangle - \left\langle \sum_{\langle x,y \rangle} s_x s_y \right\rangle^2 \right]. \end{aligned} \tag{16}$$

In the case of films, we consider the reduced free energy per area,

$$f = -\frac{1}{L_1 L_2} \ln Z \tag{17}$$

and the energy per area,

$$E = \frac{1}{L_1 L_2}\frac{\partial \ln Z}{\partial \beta} = \frac{1}{L_1 L_2}\left\langle \sum_{\langle x,y\rangle} s_x s_y \right\rangle. \tag{18}$$

C. The magnetization profile of films

The film is invariant under translations in the 1 and 2 direction of the lattice. Therefore the magnetization only depends on x_0 and we can average over x_1 and x_2:

$$m(x_0) = \frac{1}{L^2}\sum_{x_1,x_2}\langle s_x\rangle. \tag{19}$$

Since the film is symmetric for $++$ boundary conditions and antisymmetric for $+-$ boundary conditions under reflections at the middle of the film, $m(x_0) = m(L_0 - x_0 + 1)$ for $++$ boundary conditions and $m(x_0) = -m(L_0 - x_0 + 1)$ for $+-$ boundary conditions.

D. The correlation length

The exponential correlation length ξ of the bulk system is defined by the decay of the slice-slice correlation function

$$G(r) \simeq c\exp(-r/\xi) \tag{20}$$

for large distances r. The slice-slice correlation function is defined as

$$G(r) = \langle S(x_0)S(x_0 + r)\rangle, \tag{21}$$

where

$$S(x_0) = \frac{1}{\sqrt{L_1 L_2}}\sum_{x_1,x_2}\left(s_{x_0,x_1,x_2} - \langle m\rangle\right), \tag{22}$$

where $\langle m\rangle$ is the bulk magnetization that vanishes in the high-temperature phase for a vanishing external field. For a detailed discussion of the second-moment correlation length defined for films, see Sec. III C of Ref. 28.

E. Monte Carlo algorithms

In the case of the Ising model, we simulated films with $L_0 \leqslant 68$ using a local Metropolis algorithm and a multispin coding implementation. We used the same program, up to small modifications, to implement the boundary conditions, as discussed in Sec. 3 in Ref. 35. On one core of an Intel(tm) Xeon(tm) E5520 CPU running at 2.27 GHz the program achieves 1.9×10^9 spin updates per second. This is about 100 times faster than on the fastest workstation that was available to us in 1993. Most simulations were performed on Quad-Core AMD Opteron(tm) 2378 CPUs running at 2.4 GHz. Here, the program achieves 1.4×10^9 spin updates per second on one core. In relation with Sec. V, we simulated films with $++$ boundary conditions with $L_0 > 68$. These were simulated by using a special version of the cluster algorithm as discussed in Ref. 28. In the case of the Blume-Capel model, we simulated the films using the same algorithms as discussed in Sec. V of Ref. 28.

Mostly we simulated lattices with periodic boundary conditions in all directions with the single-cluster algorithm[36] in the case of the Ising model and a hybrid[37] of the local heat-bath and the single-cluster algorithm in the case of the Blume-Capel model.

In all our simulations, we used the Mersenne twister algorithm[38] as a pseudorandom number generator. In total, our simulations took the equivalent of about 50 years of CPU time on a single core of a Quad-Core AMD Opteron(tm) Processor 2378 running at 2.4 GHz.

III. FINITE SIZE SCALING AND CORRECTIONS TO SCALING

The reduced excess free energy per area of a film is given by

$$f_{\rm ex}(L_0,\beta) = f(L_0,\beta) - L_0 f_{\rm bulk}(\beta). \tag{23}$$

In the reduced excess free energy, the analytic bulk contribution cancels. Therefore it can be written as

$$f_{\rm ex}(L_0,\beta) = f_{{\rm ex},s}(L_0,\beta) + 2f_r(\beta), \tag{24}$$

where $f_{{\rm ex},s}$ is the singular part and f_r is an analytic contribution due to the boundaries. In the absence of an external field, this contribution is the same for a boundary where all spins are fixed to $+1$ and one where all spins are fixed to -1. The free energy of a system is conserved under renormalization group transformations. Therefore the singular part of the reduced excess free energy behaves as

$$f_{ex,s}(L_0,\beta) = L_0^{-2}H[t(L_0/\xi_0)^{y_t}, bL_0^{y_1},\dots], \tag{25}$$

where $y_t = 1/\nu$ and $y_1 = -\omega$ are the thermal and the leading irrelevant renormalization group exponents, respectively. Expanding the universal scaling function $H(x,u,\dots)$ in u around $u = 0$, we arrive at

$$f_{{\rm ex},s}(L_0,\beta) = L_0^{-2}h(x)\left[1 + b\ p(x)L_0^{-\omega} + \dots\right], \tag{26}$$

where $x = t(L_0/\xi_0)^{1/\nu}$ and the leading correction is characterized by the universal function $p(x)$. Taking minus the derivative with respect to L_0, we get the thermodynamic Casimir force

$$\begin{aligned}\frac{1}{k_b T}F_{\rm Casimir} &= L_0^{-3}\theta(x)\Bigg(1 + b\left\{p(x) + \frac{h(x)}{\theta(x)}\left[\omega p(x)\right.\right.\\ &\left.\left. - \frac{x}{\nu}p'(x)\right]\right\}L_0^{-\omega} + \dots\Bigg),\end{aligned} \tag{27}$$

where

$$\theta(x) = 2h(x) - \frac{x}{\nu}h'(x). \tag{28}$$

Note that at the critical point $\theta(0) = 2h(0)$. In the literature, $h(0)$ is called Casimir amplitude and is denoted by Δ. Also note that

$$\theta'(0) = \left(2 - \frac{1}{\nu}\right)h'(0). \tag{29}$$

Taking minus the derivative with respect to β, we get

$$E_{\rm ex}(L_0,\beta) = L_0^{-2}[L_0/\xi_0]^{1/\nu} h'(x) \times \left\{1 + b\left[p(x) + \frac{h(x)p'(x)}{h'(x)}\right] L_0^{-\omega} + \ldots\right\} - 2f_r'(\beta). \quad (30)$$

IV. FINITE SIZE SCALING AT THE CRITICAL POINT

First, we study finite size scaling at the critical point, i.e., $x = t(L_0/\xi_0)^{1/\nu} = 0$. To this end, we analyze data for the free energy difference between films with $+-$ and $++$ boundary conditions, the energy density and the magnetization profile for both types of boundary conditions. Finally, we also consider the second moment correlation length for $+-$ boundary conditions.

For a given quantity, at a given value of x, it is a trivial recast to express corrections to scaling in the form (8). The nontrivial question that we investigate here is whether leading corrections in different quantities can be expressed by the same or at least similar effective thicknesses $L_{0,\rm eff}$.

In the *Ansätze* below, we shall use in addition to Eq. (8),

$$L_{0,\rm eff} = L_0 + L_s + c(L_0 + L_s)^{-\omega} + d(L_0 + L_s)^{-\epsilon} \quad (31)$$

in order to probe for the effect of subleading corrections. As discussed in Intoduction, there are infinitely many subleading corrections starting with $\epsilon = 2\omega \approx \omega'$, $1 + \omega$, and $\omega'' \approx 2$. Given the accuracy of our data, it is only possible to put one subleading correction in the *Ansätze*. In the following, we shall take either $\epsilon = 1.664$ or $\epsilon = 2$. Fitting with *Ansätze* that only approximate the behavior of the data, one has to be aware of systematic errors. In the literature, it is often implicitly assumed that an acceptable χ^2/d.o.f. means that such systematic errors are small and of a similar size or even smaller than the statistical errors of the fit parameters. However, this is definitely not the case. The severity of the problem depends of course on the type of the approximation and the range of the data that are available. Below, we shall see that the differences between results of fits with Eq. (8) and ones with Eq. (31) are, e.g., five times larger than the statistical error. The error that we quote for final results is chosen such that both the results of fits with Eqs. (8) and (31) are covered.

A. The difference of free energies per area between $+-$ and $++$ boundary conditions

First, we studied the difference

$$D_{f,+-,++}(L_0,\beta) = f_{+-}(L_0,\beta) - f_{++}(L_0,\beta), \quad (32)$$

where f_{+-} and f_{++} are the reduced free energies for $+-$ and $++$ boundary conditions, respectively. In this difference, the surface and the bulk contributions exactly cancel and therefore at the critical point,

$$D_{f,+-,++}(L_0,\beta_c) \simeq (\Delta_{+-} - \Delta_{++})\, L_0^{-2}, \quad (33)$$

where Δ_{+-} and Δ_{++} are the Casimir amplitudes for $+-$ and $++$ boundary conditions, respectively. Similar to the case of periodic and antiperiodic boundary conditions,[39,40] the ratio Z_{+-}/Z_{++} of partition functions can be directly computed by using the cluster algorithm. To this end, one determines for $++$ boundary conditions the fraction of cluster decompositions where the two boundaries do not belong to the same cluster. These cluster decompositions would allow to update to $+-$ boundary conditions. Since for $+-$ boundary conditions the update to $++$ boundary conditions is always allowed, the fraction discussed above is an estimate of Z_{+-}/Z_{++}.

Unfortunately, at the critical point, for $L \gg L_0$, the ratio Z_{+-}/Z_{++} is far too small to allow for an efficient sampling. Therefore we simulated in the high-temperature phase at $\beta = \beta_0$ such that $L_0/\xi(\beta_0) \approx 6$, where ξ is the bulk correlation length. Here, for $L = 4L_0$, which we used in our simulations, the value of Z_{+-}/Z_{++} is a few percent. In order to get $f_{+-} - f_{++}$ at larger values of β, in particular, at the critical point, we performed an integration of energy differences:

$$D_{f,+-,++}(L_0,\beta) = D_{f,+-,++}(L_0,\beta_0) - \int_{\beta_0}^{\beta} {\rm d}\tilde\beta\; D_{E,+-,++}(L_0,\tilde\beta), \quad (34)$$

where $D_{E,+-,++} = E_{+-} - E_{++}$. We performed this integration numerically, using the trapezoidal rule. To this end, we used at least 36 values of β between β_0 and β_c as nodes. For a detailed discussion of the corresponding Monte Carlo simulations, see Sec. VI below. In most cases, we used the same data as discussed in Sec. VI. Only for the Ising model at the thicknesses $L_0 = 24$ and 48 and the Blume-Capel model at the thickness $L_0 = 68$, we performed additional simulations. For an analytic integrand, the estimate obtained by using the trapezoidal rule behaves as $I(h) = I(0) + ah^2 + O(h^4)$, where $I(0)$ is the integral to be computed and h is the step size. We estimated the systematic error by computing $I(2h)$, i.e., performing the integration (34) with half of the available data points. The systematic error is then estimated by $\epsilon = [I(2h) - I(h)]/3$. It turned out that the systematic error ϵ is considerably larger than the rather small statistical error. Therefore we extrapolated our result as $I(0) = I(h) - [I(2h) - I(h)]/3 + O(h^4)$. In the case of the Blume-Capel model and $L_0 = 34$, where we simulated at 116 values of β between β_0 and β_c, we checked the efficiency of the extrapolation by computing $I(h)$, $I(2h)$, and $I(4h)$. We found agreement between $I(h) - [I(2h) - I(h)]/3$ and $I(2h) - [I(4h) - I(2h)]/3$ within the statistical error. In Table I, we summarized our numerical results for the critical point.

We fitted the data obtained for the Ising model with the *Ansätze*

$$D_{f,+-,++} = \Delta\,[L_0 + L_s + c(L_0 + L_s)^{1-\omega}]^{-2} \quad (35)$$

and

$$D_{f,+-,++} = \Delta\,[L_0 + L_s + c(L_0 + L_s)^{1-\omega} + d(L_0 + L_s)^{1-\epsilon}]^{-2}, \quad (36)$$

where we set either $\epsilon = 1.664$ or $\epsilon = 2$.

Fitting with the *Ansatz* (35), setting $\omega = 0.832$, we get for $L_{0,\rm min} = 16$ the result $\Delta = 3.1987(9)$, $c = 1.429(12)$, $L_s = 1.043(12)$, and χ^2/d.o.f.$= 1.20$. Note that all data with $L_0 \geqslant L_{0,\rm min}$ are taken into account in the fit. Instead,

TABLE I. We give the difference $D_{f,+-,+-}$ of the reduced free energies per area between $+-$ and $++$ boundary conditions at our estimates of the inverse critical temperature, i.e., $\beta = 0.22165462$ for the Ising model and $\beta = 0.387721735$ for the Blume-Capel model at $D = 0.655$.

L_0	Model	$D_{f,+-,+-}$
14	I	0.01069953(37)
15	I	0.00953606(25)
16	I	0.00855417(15)
17	I	0.00771682(12)
24	I	0.00423239(15)
32	I	0.002522796(50)
34	I	0.002258418(55)
48	I	0.00119288(10)
64	I	0.000693495(64)
68	I	0.000617863(63)
16	BC	0.00999910(67)
17	BC	0.00897065(65)
32	BC	0.00279016(11)
34	BC	0.00248788(11)
68	BC	0.00065641(11)

taking $\omega = 0.826$, we get $\Delta = 3.1995(9)$, $c = 1.367(11)$, $L_s = 1.100(15)$, and χ^2/d.o.f.$= 1.20$. This means that the estimate of Δ depends little on the value of ω, while c and L_s are quite sensitive to it. We redid these fits for $D_{f,+-,++}$ evaluated at $\beta = 0.2216546$. The results change only by little.

Next, we fitted all data, i.e., $L_{0,\min} = 14$, with the *Ansatz* (36). We get, fixing $\omega = 0.832$ and $\epsilon = 1.664$, the results $\Delta = 3.2025(21)$, $c = 1.57(6)$, $L_s = 0.78(11)$, $d = 0.35(14)$, and χ^2/d.o.f.$= 1.47$. Instead, for $\epsilon = 2$, we get $\Delta = 3.2016(19)$, $c = 1.52(4)$, $L_s = 0.88(7)$, $d = 1.52(4)$, and χ^2/d.o.f.$= 1.45$. We see that by adding a subleading correction, the estimate of Δ changes little, while the results for c and L_s are considerably shifted. Note that the estimates of c and L_s are highly anticorrelated. The resulting $L_{0,\text{eff}}$, Eq. (8), for the thicknesses analyzed here, depend much less on the *Ansatz* that is used. Taking all fits discussed above into account, we conclude

$$\Delta_{+-} - \Delta_{++} = 3.200(5). \tag{37}$$

Next, we fitted our data for the Blume-Capel model with the *Ansätze*

$$D_{f,+-,++} = \Delta\,(L_0 + L_s)^{-2} \tag{38}$$

and

$$D_{f,+-,++} = \Delta\,[L_0 + L_s + d(L_0 + L_s)^{-1}]^{-2}. \tag{39}$$

Fitting all data with the *Ansatz* (38), we get $\Delta = 3.20901(25)$, $L_s = 1.9140(11)$, and χ^2/d.o.f. $= 1.12$. Fitting all data with the *Ansatz* (39), we get $D = 3.2071(5)$, $L_s = 1.898(4)$, $d = 0.20(6)$, and χ^2/d.o.f. $= 0.72$, instead. We redid these fits for $D_{f,+-,++}$ evaluated at $\beta = 0.38772176$ in order to estimate the error due to the uncertainty of β_c. Finally, in order to check for the possible effect of residual corrections to scaling $\propto L_0^{-\omega}$, we fitted our data with the *Ansätze* (35) and (36), where we fixed the amplitude of the leading correction to $c = 1.5/30$. Note that in Ref. 7, we found that the amplitudes of the leading correction are at least suppressed by the factor $1/30$ in the Blume-Capel model at $D = 0.655$ compared with the spin-$1/2$ Ising model.

Taking these fits into account, we arrive at

$$\Delta_{+-} - \Delta_{++} = 3.208(5), \tag{40}$$

which is consistent with the estimate (37) obtained above. Furthermore, these results are fully consistent with $\Delta_{+-} - \Delta_{++} = [\theta_{+-}(0) - \theta_{++}(0)]/2 = [5.613(20) + 0.820(15)]/2 = 3.217(18)$ obtained in Sec. VI C in Ref. 28. Our result is slightly larger than $\Delta_{+-} - \Delta_{++} = 2.71(2) - 0.376(29) = 3.09(5)$, which the authors obtained by fitting their data for the thermodynamic Casimir force per area with *Ansatz* (26) in Ref. 24. In Ref. 30, the authors used different *Ansätze*. Equations (17), (18), and (19) coincide at the critical point with our *Ansatz* (7). The authors argue that corrections $\propto L_0^{-\omega}$ are effectively taken into account by the $\propto L_0^{-1}$ correction that is present in the *Ansatz*. In Fig. 6(a) in Ref. 30, we see that their strong symmetry breaking results, i.e., $\tilde{h}_1 = -100$ and $\tilde{h}_1 = 100$ clearly deviate from ours.[28] To understand this discrepancy, we fitted our data for the Ising model with *Ansatz* (39). Fitting all our data we get $\Delta = 3.1467(4)$, $L_s = 3.480(4)$, $d = -5.83(5)$, and χ^2/d.o.f.$= 76.35$. Fitting only the data with $L_0 \leqslant 34$ and assuming a statistical error that is 3 times larger than the one that we actually achieved, we get $\Delta = 3.136(2)$, $L_s = 3.39(2)$, $d = -4.7(2)$, and χ^2/d.o.f.$= 1.03$. While χ^2/d.o.f.≈ 1, this is completely incompatible with our final result (37), which substantiates our statements above on fitting with approximate *Ansätze*.

Finally, note that our results for L_s of the Blume-Capel model at $D = 0.655$ are fully consistent with $L_s = 1.9(1)$,[28] $L_s = 2l_{\text{ex}} = 1.92(4)$, and $L_s = 1.90(5)$.[31] In Sec. VI below, we shall assume $L_s = 1.91(5)$.

B. Simulations at the critical point

In order to compute the energy per area and the magnetization profile at the critical point of the Ising model, we performed high statistics simulations at $\beta = 0.2216546$, which was our estimate of β_c when we started the simulations. In order to obtain the observables at $\beta = 0.22165462$, we computed the derivative of the observables with respect to β from finite differences. In Table II, we summarize the lattice sizes and the statistics of our first set of simulations. In a second set of simulations with $+-$ boundary conditions, we measured the second moment correlation length in addition. We simulated lattices of the thicknesses $L_0 = 24$, 32, 48, 64, and 96. The number of measurements is 51.2×10^7, 51.9×10^7, 49.1×10^7, 34.6×10^7, and 7.8×10^7, respectively. Also here, we performed 16 sweeps with the Metropolis algorithm for each measurement. For this second set of simulations, $L = 4L_0$. For $L_0 = 6$, we simulated $L = 12$, 14, 16, 18, 20, 24, 36, 48, and 60 performing 6.4×10^8 measurements throughout. From the analysis of these runs, we conclude that for $+-$ boundary conditions, at the critical point, $L = 4L_0$ is fully sufficient to keep deviations from the $L \to \infty$ limit at a negligible level. In our simulations, we wrote averages over 64 000 measurements on disk to keep the amount of data tractable. In order to estimate autocorrelation times, we

TABLE II. Number of measurements (stat) in our simulations of the Ising model at $\beta = 0.2216546$. For each measurement, 16 sweeps with the Metropolis algorithm were performed. In these simulations, $L = 6L_0$ and $L = 10L_0$ for $++$ and $+-$ boundary conditions, respectively.

L_0	stat $++$	stat $+-$
6	64.0×10^8	64.0×10^7
7	57.2×10^8	64.0×10^7
8	45.3×10^8	64.0×10^7
9	47.9×10^8	64.0×10^7
10	39.4×10^8	51.5×10^7
11	31.4×10^8	46.1×10^7
12	24.0×10^8	44.8×10^7
13	15.1×10^8	37.9×10^7
14	15.5×10^8	32.4×10^7
15	15.3×10^8	27.8×10^7
16	14.2×10^8	25.6×10^7
17	10.4×10^8	21.5×10^7
18	10.9×10^8	19.5×10^7
19	11.8×10^8	18.9×10^7
20	10.4×10^8	18.8×10^7
22	10.4×10^8	28.7×10^7
24	67.1×10^7	20.4×10^7
26	64.3×10^7	22.7×10^7
28	62.0×10^7	25.8×10^7
32	62.9×10^7	22.5×10^7
36	31.5×10^7	22.7×10^7
48	14.4×10^7	2.9×10^7
64	9.9×10^7	2.7×10^7

did a few additional simulations, where every measurement was stored. For example, we performed 10^5 measurements for $+-$ boundary conditions, $L_0 = 96$ and $L = 384$. From this run, we got the integrated autocorrelation times $\tau_{\rm int} = 3.3(2)$, 15.2(1.0), and 28.(3.) in units of measurements for the energy per area, the magnetic susceptibility, and the magnetisation in the middle of the film. The autocorrelation times of a local algorithm grow like $\tau \propto L_0^z$ at the critical point, where $z \approx 2$. Therefore despite the efficient multispin coding implementation of the Metropolis algorithm, the cluster algorithm should become more efficient starting from a certain thickness L_0. Since $\tau_{\rm int}$ enters into the statistical error, this thickness depends to some extend on the observable one is interested in. For lack of human time, we did not systematically investigate these questions.

C. The energy per area

Taking Eq. (30) at $x = 0$ and ignoring corrections to scaling, we arrive at

$$E_{\rm ex}(L_0,\beta_c) = B + aL_0^{-2+1/\nu}, \tag{41}$$

where $B = 2f_r(\beta_c)$ and $a = \xi_0^{-1/\nu} h'(0)$.

In order to compute the excess energy, we used the estimate of $E_{\rm bulk}(\beta_c)$, Eq. (A4), obtained in Appendix A 1. Replacing L_0 by $L_{0,\rm eff}$ in Eq. (41), we arrive at the *Ansätze*

$$E_{\rm ex}(L_0,\beta_c) = B + a[L_0 + L_s + c(L_0 + L_s)^{1-\omega}]^{-2+1/\nu} \tag{42}$$

and

$$E_{\rm ex}(L_0,\beta_c) = B + a[L_0 + L_s + c(L_0 + L_s)^{1-\omega} + d(L_0 + L_s)^{1-\epsilon}]^{-2+1/\nu}, \tag{43}$$

where we set either $\epsilon = 1.664$ or $\epsilon = 2$. In our fits, B, a, c, L_s, and d are free parameters. We fixed $\nu = 0.63002$ and $\omega = 0.832$.

First, we analyzed our data for $+-$ boundary conditions. Fitting with the *Ansatz* (42), we get an acceptable χ^2/d.o.f. starting from $L_{0,\rm min} = 18$. For $L_{0,\rm min} = 20$, we get $B = 7.8010(7)$, $a = -15.455(7)$, $c = 1.472(35)$, $L_s = 1.413(44)$, and χ^2/d.o.f. $= 0.62$. Using the *Ansatz* (43), we get an acceptable χ^2/d.o.f. already for $L_{0,\rm min} = 7$ both for $\epsilon = 1.664$ and $\epsilon = 2$. For example, for $L_{0,\rm min} = 8$ and $\epsilon = 1.664$, we get $B = 7.80405(23)$, $a = -15.4946(19)$, $c = 2.028(8)$, $L_s = 0.476(10)$, $d = -0.27(4)$, and χ^2/d.o.f. $= 0.93$. Instead, for $L_{0,\rm min} = 8$ and $\epsilon = 2$, we get $B = 7.80279(25)$, $a = -15.4790(20)$, $c = 1.794(9)$, $L_s = 0.903(11)$, $d = 0.13(4)$, and χ^2/d.o.f. $= 1.13$. We see that the results depend strongly on the *Ansätze* that is used. This holds, in particular, for the estimates of c and L_s. We redid the fits using shifted values of the input parameters to estimate the error of our results due to the uncertainty of these parameters. Taking into account the results of all these fits, we arrive at $B = 7.803(5)$ and

$$a_{I,+-} = -15.48(5) - 130(\nu - 0.63002), \tag{44}$$

where for a_{+-}, we give the dependence on the value of ν explicitly. The error induced by the uncertainty of the other input parameters is included into the number given in ().

For $++$ boundary conditions fitting with, the *Ansätze* (42) gives acceptable values of χ^2/d.o.f. already for $L_{0,\rm min} = 7$. For example, for $L_{0,\rm min} = 8$, we get $B = 7.80168(22)$, $a = -10.2105(16)$, $c = 1.462(7)$, $L_s = 1.16(7)$, and χ^2/d.o.f. $= 1.23$. Instead, fitting with the *Ansatz* (43), we get for $\epsilon = 1.664$ and $L_{0,\rm min} = 8$ the result $B = 7.8054(7)$, $a = -10.248(6)$, $c = 2.02(4)$, $L_s = 0.27(5)$, $d = 2.3(4)$, and χ^2/d.o.f. $= 1.02$. Fixing $\epsilon = 2$, we get results that lie between those of the two fits discussed before. Also in the case of $++$ boundary conditions, we redid the fits with shifted values of the input parameters. As our final result, we quote $B = 7.804(5)$ and

$$a_{I,++} = -10.23(5) - 70(\nu - 0.63002). \tag{45}$$

Note that the results obtained for B with $+-$ and $++$ boundary conditions agree as theoretically expected.

Assuming $\nu = 0.63002$, we get $h'_{+-}(0) = -15.48(5) \times 0.1962(1)^{1/0.63002} = -1.167(5)$ and $h'_{++}(0) = -10.23(5) \times 0.1962(1)^{1/0.63002} = -0.771(5)$ from the analysis of the Ising model. In Ref. 28, we found for the Blume-Capel model at $D = 0.655$ the results $a_{BC,++} = -8.04(1)$ and $a_{BC,+-} = -12.18(3)$. Hence $h'_{+-}(0) = -12.18(3) \times 0.2283(1)^{1/0.63002} = 1.168(4)$ and $h'_{++}(0) = -8.04(1) \times 0.2283(1)^{1/0.63002} = -0.771(2)$. We see that the results obtained for the universal quantities $h'_{+-}(0)$ and $h'_{++}(0)$ are in perfect agreement. Using Eq. (29), we arrive at

$$\theta'_{+-}(0) = -0.482(2), \quad \theta'_{++}(0) = -0.318(2) \tag{46}$$

taking into account the results obtained from both models.

Finally, we analyzed the difference $D_{E,+-,++}$ at the critical point. The advantage of this quantity is that the bulk energy and the surface contributions exactly cancel. We fitted our data with the *Ansätze*

$$E_{\rm ex}(L_0,\beta_c) = D_a[L_0+L_s+c(L_0+L_s)^{1-\omega}]^{-2+1/\nu} \quad (47)$$

and

$$E_{\rm ex}(L_0,\beta_c) = D_a[L_0+L_s+c(L_0+L_s)^{1-\omega} + d(L_0+L_s)^{1-\epsilon}]^{-2+1/\nu}. \quad (48)$$

Fitting with the *Ansatz* (47), we get an acceptable χ^2/d.o.f. only for rather large values of $L_{0,\rm min}$. For example, for $L_{0,\rm min}=26$, we get $D_a=-5.2548(19)$, $c=1.80(10)$, $L_s=1.49(14)$, and χ^2/d.o.f. $=1.26$. Fitting with the *Ansatz* (48) and $\epsilon=1.644$, we get for $L_{0,\rm min}=12$, the results $D_a=-5.2570(8)$, $c=2.15(4)$, $L_s=0.81(5)$, $d=-3.56(18)$, and χ^2/d.o.f. $=1.04$. Instead, for $\epsilon=2$, we get $D_a=-5.2548(7)$, $c=1.92(3)$, $L_s=1.25(4)$, $d=-3.71(16)$, and χ^2/d.o.f. $=1.09$. Also here, we redid the fits with shifted values of the input parameters. We arrive at the final result

$$a_{I,+-}-a_{I,++} = -5.256(4)-75(\nu-0.63002). \quad (49)$$

D. The magnetization profile

For simplicity, we shall not study the complete magnetization profile, but we shall restrict ourselves on the magnetization in the middle of the film and the slope of the magnetization in the middle of the film for $++$ and $+-$ boundary conditions, respectively. Let us first discuss the case of $++$ boundary conditions. The magnetisation in the middle of the film at the critical point behaves as

$$m_{\rm mid} = C_m L_0^{-\beta/\nu}. \quad (50)$$

The amplitude C_m is not universal, but one can construct universal amplitude ratios that combine C_m with the amplitude of the bulk correlation length and the bulk magnetization or the magnetic susceptibility. Here, we only intend to compare our result for $C_{m,I}$ for the Ising model with $C_{m,\rm BC}$ obtained previously for the Blume-Capel model at $D=0.655$.[28] To this end, it is sufficient to determine the relative normalization of the magnetization between these two models. To this end, we compare the magnetic susceptibility of systems with the extension $L_0=L_1=L_2$ and periodic boundary conditions in all three directions that we computed in relation with Ref. 7. In particular, we fitted the data for the magnetic susceptibility at $Z_a/Z_p=0.5425$ with the *Ansatz*

$$\bar\chi = C_\chi L^{2-\eta}(1+cL^{-\omega})+b, \quad (51)$$

where we fixed $\eta=0.03627(10)$ and $\omega=0.832(6)$. We arrive at

$$\sqrt{\frac{C_{\chi,I}}{C_{\chi,\rm BC}}} = 1.2811(2), \quad (52)$$

where statistical and systematical errors as well as the uncertainty of η and ω are taken into account.

In order to define the magnetization in the middle of the film for even values of the thickness L_0, we quadratically extrapolated the magnetizations of the slice that is next to the middle and the one that is next to next. We fitted these data with the *Ansätze*

$$m_{\rm mid} = C_m[L_0+L_s+c(L_0+L_s)^{1-\omega}]^{-\beta/\nu} \quad (53)$$

and

$$m_{\rm mid} = C_m[L_0+L_s+c(L_0+L_s)^{1-\omega} + d(L_0+L_s)^{1-\epsilon}]^{-\beta/\nu}, \quad (54)$$

where we fixed $\beta/\nu=(1+\eta)=0.5018135$, $\omega=0.832$, and $\epsilon=1.664$ or $\epsilon=2$. In the following, we only take into account data for even values of L_0. Using *Ansatz* (53), we get for $L_{0,\rm min}=24$ the results $C_m=1.71799(18)$, $c=1.63(2)$, $L_s=1.31(3)$, and χ^2/d.o.f.$=0.21$. Using *Ansatz* (54), we get with $\epsilon=2$ an acceptable χ^2/d.o.f. already for $L_{0,\rm min}=6$. For $L_{0,\rm min}=8$, we get $C_m=1.71880(7)$, $c=1.844(8)$, $L_s=0.922(11)$, $d=1.289(14)$, and χ^2/d.o.f.$=0.78$. For $\epsilon=1.664$ and $L_{0,\rm min}=10$, we get $C_m=1.71929(11)$, $c=2.016(17)$, $L_s=0.563(29)$, $d=1.172(27)$, and χ^2/d.o.f.$=0.59$.

We redid these fits using shifted values of β_c, η, and ω. As final results, we quote

$$C_{m,I} = 1.7187(10)+4.8(\eta-0.03627), \quad (55)$$

where we give explicitly the dependence of our result on the value of η.

In Ref. 28, we analyzed $m_{\rm mid}$ for the Blume-Capel model at $D=0.655$ for thicknesses up to $L_0=32$. Later,[31] we added data for $L_0=48$, 64, and 96. Taking into account also these data, we arrive at

$$C_{m,\rm BC} = 1.3421(8)+2.8(\eta-0.03627). \quad (56)$$

We get

$$\frac{C_{m,I}}{C_{m,\rm BC}} = 1.2806(16), \quad (57)$$

which is fully consistent with Eq. (52).

In the case of $+-$ boundary conditions, we consider the slope of the magnetization profile in the middle of the film. It scales as

$$S_{\rm mid} = C_s L_0^{-1-\beta/\nu}. \quad (58)$$

We fitted our data for the Ising model with the *Ansätze*

$$S_{\rm mid} = C_s[L_0+L_s+c(L_0+L_s)^{1-\omega}]^{-1-\beta/\nu} \quad (59)$$

and

$$S_{\rm mid} = C_s[L_0+L_s+c(L_0+L_s)^{1-\omega} + d(L_0+L_s)^{1-\epsilon}]^{-1-\beta/\nu}, \quad (60)$$

where we fixed $\eta=0.03627$, $\omega=0.832$, and $\epsilon=1.664$ or $\epsilon=2$. Also here, we fitted only the data for even values of L_0. Fitting with the *Ansatz* (59), we find small values of χ^2/d.o.f. already for $L_{0,\rm min}=8$. For $L_{0,\rm min}=10$, we get $C_{s,I}=7.2013(4)$, $c=1.4603(25)$, $L_s=0.7023(31)$, and χ^2/d.o.f.$=0.39$. Fitting with the *Ansatz* (60), we find that the parameter d vanishes within the error bars. Taking into account the error due to the uncertainty of the input parameters ω and η, we arrive at the

$$C_{s,I} = 7.201(3)+19(\eta-0.03627). \quad (61)$$

TABLE III. In the second column, we give the second moment correlation length obtained from simulations of lattices with $L = 4L_0$ for $+-$ boundary conditions at the critical point of the Ising model. In the third column, we give $L_{\rm ex} = L_{0,\rm eff} - L_0$. For the definition of $L_{0,\rm eff}$ see the text. In the fourth, fifth, sixth, and seventh column, we give $L_{\rm ex} = L_{0,\rm eff} - L_0$ derived from $D_{f,+-,++}$, $D_{E,+-,++}$, $m_{\rm mid}$, and $S_{\rm mid}$, respectively.

L_0	$\xi_{\rm 2nd}$	$L_{\rm ex}$, $\xi_{\rm 2nd}$	$L_{\rm ex}$, $D_{f,+-,++}$	$L_{\rm ex}$, $D_{E,+-,++}$	$L_{\rm ex}$, $m_{\rm mid}$	$L_{\rm ex}$, $S_{\rm mid}$
24	5.6881(24)	2.89[10]	3.51[2]	4.61[10]	4.14[3]	3.20[1]
32	7.4025(42)	3.00[13]	3.64[3]	4.76[12]	4.27[4]	3.32[1]
48	10.807(10)	3.10[19]	3.83[4]	4.99[16]	4.49[6]	3.51[1]
64	14.204(20)	3.16[25]	3.97[5]	5.16[20]	4.65[8]	3.64[2]
96	20.99(10)	3.2[4]	...	...	...	3.85[3]

Fitting data obtained in relation with Ref. 28 for the Blume-Capel model, we get

$$C_{s,\rm BC} = 5.625(10) + 10(\eta - 0.03627). \tag{62}$$

We get

$$\frac{C_{s,I}}{C_{s,\rm BC}} = 1.280(3), \tag{63}$$

which is fully consistent with Eq. (52).

E. The correlation length

Finally, we discuss the second-moment correlation length of films with $+-$ boundary conditions at the critical point. Our numerical results are summarized in Table III. Since here we generated less data than for the quantities discussed above, we abstain from fitting the data for the correlation length. In Ref. 28, we found $\xi_{\rm 2nd} = 0.2115(8)(L_0 + L_s)$. Based on this result, we define

$$L_{0,\rm eff} = \xi_{\rm 2nd}/0.2115(8). \tag{64}$$

In the third column of Table III, we quote $L_{0,\rm eff} - L_0$. In the square brakets, we give the error due to the uncertainty of the amplitude of the correlation length of the film. For comparison, we give analogous results derived from the difference of free energies $D_{f,+-,++}$, the difference of energies $D_{E,+-,++}$, the magnetization in the middle of the film for $++$ boundary conditions and the slope of the magnetisation in the middle of the film for $+-$ boundary conditions.

We see that the values of $L_{0,\rm eff} - L_0$ computed from different observables are of a similar size. However, the differences are considerably larger than the sum of the errors. Therefore it is quite clear that $L_{0,\rm eff} - L_0$ is not exactly the same for all quantities.

V. THERMODYNAMIC CASIMIR FORCE AND THE TRANSFER MATRIX

First, let us briefly recall the discussion given in Sec. IV of Ref. 28. The partition function of a system with fixed boundary conditions can be expressed in terms of the eigenvalues of the transfer matrix and the overlap of the eigenvectors with the boundary states. Let us consider a lattice of the size $L_0 \times L^2$, where L is large compared with the bulk correlation length but still finite. We consider the transfer matrix T that acts on vectors that are build on the configurations living on L^2 slices. We denote the eigenvalues of T by λ_α and the corresponding eigenvector by $|\alpha\rangle$, where $\alpha = 0,1,2,\ldots,\alpha_{\rm max}$. The eigenvalues are ordered such that $\lambda_\alpha \geqslant \lambda_\beta$ for $\alpha < \beta$. In particular, λ_0 is the largest eigenvalue. The partition function of the system with fixed boundaries is given by

$$Z_{b_1,b_2} = \sum_\alpha \lambda_\alpha^l \, \langle b_1|\alpha\rangle\langle b_2|\alpha\rangle, \tag{65}$$

where $l = L_0 + 1$ for our definition of the thickness L_0. The boundary states $b_{1,2}$ are either $+$ or $-$ here. It follows that

$$\begin{aligned}\frac{L^2}{k_B T} F_{\rm Casimir} &= \frac{\partial}{\partial l}\left(\ln Z_{b_1,b_2} - l \ln \lambda_0\right) \\ &= \frac{\sum_\alpha \ln(\lambda_\alpha/\lambda_0)\,(\lambda_\alpha/\lambda_0)^l\,\langle b_1|\alpha\rangle\langle b_2|\alpha\rangle}{\sum_\alpha (\lambda_\alpha/\lambda_0)^l \langle b_1|\alpha\rangle\langle b_2|\alpha\rangle} \\ &= -\frac{\sum_\alpha m_\alpha \exp(-m_\alpha l)\,\langle b_1|\alpha\rangle\langle b_2|\alpha\rangle}{\sum_\alpha \exp(-m_\alpha l)\,\langle b_1|\alpha\rangle\langle b_2|\alpha\rangle},\end{aligned} \tag{66}$$

where $1/\xi_\alpha = m_\alpha = -\ln(\lambda_\alpha/\lambda_0)$ are inverse correlation lengths. In the high-temperature phase for $\xi_1 = \xi \ll L_0$, the force is dominated by the contribution from $\alpha = 1$. Hence

$$\begin{aligned}\tilde\theta(ml) &\approx \frac{l^3}{k_B T} F_{\rm Casimir} \\ &\approx -m^3 l^3 \exp(-ml)\,\frac{1}{m^2 L^2}\,\frac{\langle b_1|1\rangle\langle b_2|1\rangle}{\langle b_1|0\rangle\langle b_2|0\rangle}.\end{aligned} \tag{67}$$

The finite size scaling behavior of the thermodynamic Casimir force implies that

$$C_b = \frac{1}{mL}\,\frac{\langle b|1\rangle}{\langle b|0\rangle} \tag{68}$$

has a finite scaling limit. The state $|0\rangle$ is symmetric under the global transformation $s_x \to -s_x$ for all x in a slice, while $|1\rangle$ is antisymmetric and therefore $C = C_+ = -C_-$. Hence

$$\tilde\theta_{++}(ml) = -\tilde\theta_{+-}(ml) = -C^2\, m^3 l^3 \exp(-ml) \tag{69}$$

for sufficiently large values of ml. Since $x = t(l/\xi_0)^{1/\nu} \simeq (ml)^{1/\nu}$, it follows that

$$\theta_{++}(x) = -\theta_{+-}(x) \simeq -C^2 x^{3\nu} \exp(-x^\nu) \tag{70}$$

for sufficiently large values of x.

A. C and the magnetisation profile

In the following, we shall discuss how the overlap amplitude C^2 can be computed from the magnetisation profile of a semi-infinite system with $+$ boundary conditions and the correlation function of slice magnetizations. In terms of the

transfer matrix, the magnetization at position x_0 in a film of thickness L_0 is given by

$$\langle M(x_0)\rangle = \left\langle \sum_{x_1,x_2} s_{x_0,x_1,x_2} \right\rangle = \frac{\sum_{\alpha,\beta} \lambda_\alpha^{x_0} \lambda_\beta^{l-x_0} \langle b_1|\alpha\rangle\langle\alpha|\hat{M}|\beta\rangle\langle\beta|b_2\rangle}{\sum_\alpha \lambda_\alpha^l \langle b_1|\alpha\rangle\langle\alpha|b_2\rangle}. \quad (71)$$

In the basis of slice configurations, $\hat{M}$ is a diagonal matrix, where the elements give the magnetization of the corresponding configuration. For $l \gg \xi$ and $\xi_2 \ll x_0 \ll l$, Eq. (71) reduces to

$$\langle M(x_0)\rangle = \frac{\lambda_1^{x_0}\lambda_0^{l-x_0}\langle b_1|1\rangle\langle 1|\hat{M}|0\rangle\langle 0|b_2\rangle}{\lambda_0^l\langle b_1|0\rangle\langle 0|b_2\rangle} = \frac{\langle b_1|1\rangle}{\langle b_1|0\rangle}\langle 1|\hat{M}|0\rangle\left(\frac{\lambda_1}{\lambda_0}\right)^{x_0} = mL\ C_{b_1}\ \langle 1|\hat{M}|0\rangle\ \exp(-mx_0). \quad (72)$$

The quantity $O_M = \langle 1|\hat{M}|0\rangle/L$ is finite in the limit $L \to \infty$, since $\langle M(x_0)\rangle/L^2$ is finite in this limit.

The slice-slice correlation function for a lattice of linear size L_0 and periodic boundary conditions is given by

$$G(r) = \frac{1}{L^2}\langle M(x_0)M(x_0+r)\rangle = \frac{1}{L^2}\frac{\sum_{\alpha,\beta}\langle\beta|\hat{M}|\alpha\rangle\langle\alpha|\hat{M}|\beta\rangle\lambda_\alpha^r\lambda_\beta^{L_0-r}}{\sum_\alpha \lambda_\alpha^{L_0}}. \quad (73)$$

Since $\hat{M}$ is antisymmetric under $s_x \to -s_x$ for all x in the slice, $\langle 0|\hat{M}|0\rangle$ vanishes. For $\xi_2 \ll x_0 \ll L_0$, we get

$$G(r) = \frac{1}{L^2}\langle 0|\hat{M}|1\rangle\langle 1|\hat{M}|0\rangle\exp(-mr) = O_M^2\exp(-mr). \quad (74)$$

Taking into account the periodicity of the lattice, we arrive at

$$G(r) = O_M^2\frac{\exp(-mr)+\exp[-m(L_0-r)]}{1+\exp(-mL_0)}, \quad (75)$$

which we shall use in our numerical analysis below.

B. Numerical implementation

In order to compute $G(r)$, we simulated lattices with $L_0 = L_1 = L_2 = L$ and periodic boundary conditions. In the case of the Blume-Capel model, we simulated the model by using a hybrid[37] of the local heat-bath and single-cluster algorithms.[36] In the case of the Ising model, we only used the single-cluster algorithm. We measured the correlation function $G(r)$ by using its cluster-improved estimator. In order to keep deviations from the thermodynamic limit negligible, we chose $L > 10\xi$ throughout. For a discussion of this point see Sec. III or Ref. 33. In order to compute ξ and O_M^2 from Eq. (75), we took the correlation function at the distance $r-1$ and r. For Eq. (74), one gets $\xi = 1/\ln[G(r)/G(r-1)]$ and $O_M^2 = G(r)\exp(r/\xi)$. For Eq. (75), we solved the system of two equations numerically. We computed the statistical errors of ξ and O_M^2 and their covariance by using the Jackknife method. We checked which distance r is needed to keep corrections due to eigenstates of the transfer matrix with $\alpha > 1$ negligible. As a result, we took $r \approx 2\xi$ throughout.

In the case of the Blume-Capel model at $D = 0.655$, we simulated at 11 values of β between $\beta = 0.34$, where $\xi = 1.50420(13)$, and $\beta = 0.3872$, where $\xi = 26.7102(16)$. For $\beta = 0.3872$, we performed about 10^7 update cycles. Each cycle consists of two sweeps of the local heat-bath algorithm and 10^4 single-cluster updates. Note that the average cluster size at $\beta = 0.3872$ is 1645.58(17), and hence the lattice of the size 270^3 is covered on average 0.84 times by these 10^4 clusters. The simulation at $\beta = 0.3872$ took the equivalent of about 13 month of CPU-time on a single core of a Quad-Core AMD Opteron(tm) Processor 2378 running at 2.4 GHz. In the case of the Ising model, we simulated at 59 values of β between $\beta = 0.125$, where $\xi = 0.667308(53)$, and $\beta = 0.2208$, where $\xi = 16.6711(12)$.

Next, we analyzed the magnetization profile of films with $++$ boundary conditions. Also, here we required that $L_i > 10\xi$. When possible, we used the results obtained from the simulations that we performed to compute the thermodynamic Casimir force. For values of β where this is not the case, we performed extra simulations using the cluster algorithm. Taking O_M^2 and ξ obtained above from the simulations of the lattices with periodic boundary conditions as input, one gets an estimate of $C(\xi)$ from Eq. (72) for each distance x_0 from the boundary. Throughout, we took our final result from $x_0 \approx 3\xi$.

In Fig. 1, we plot our results for $C(\xi)$ as a function of $m = 1/\xi$ for the Ising model and the Blume-Capel model at $D = 0.655$. Note that the error bars are much smaller than the size of the symbols. For example, for the Blume-Capel model at $\beta = 0.3872$, we obtain $C(\xi) = 1.2241(4)$ and for the Ising model at $\beta = 0.2208$, we get $C(\xi) = 1.1500(3)$. The data for the Blume-Capel model essentially fall on a straight line, confirming that corrections $\propto\xi^{-\omega}$ are eliminated and those $\propto\xi^{-1}$ caused by the boundary dominate. In contrast, for the Ising model, we see a clear bending of the curve. It is conceivable that in the limit $\xi \to \infty$, the two curves converge to a unique value.

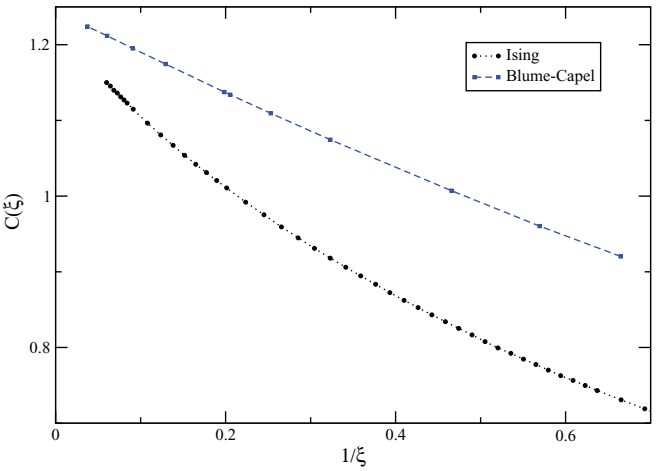

FIG. 1. (Color online) The amplitude $C(\xi)$ for the Ising and the Blume-Capel models at $D = 0.655$ as a function of $1/\xi$.

In order to substantiate these qualitative observations, we fitted our data with the *Ansätze*

$$C(\xi) = C\exp(-c/\xi) \tag{76}$$

and

$$C(\xi) = C\exp(-c/\xi) + a\xi^{-\epsilon}, \tag{77}$$

where C, c and a are the parameters of the fit. First, we analyzed our data for the Blume-Capel model. Fitting with the *Ansatz* (76), we get $\chi^2/\text{d.o.f.} = 0.67$, for fitting all data except the smallest value of β. The results for the parameters of the fit are $C = 1.24568(21)$ and $c = 0.4572(7)$. Next, we fitted all data with the *Ansatz* (77). Fixing $\epsilon = 0.832$, we get $C = 1.2462(5)$, $c = 0.442(9)$, $a = -0.017(11)$, and $\chi^2/\text{d.o.f.} = 1.06$. For $\epsilon = 2$, we get $C = 1.24588(27)$, $c = 0.4591(15)$, $a = 0.0043(23)$, and $\chi^2/\text{d.o.f.} = 0.64$. As our final estimate, we give

$$C = 1.2459(7), \tag{78}$$

where the error bar covers the results of the three fits given above. The estimate $C^2 = 1.5(1)$ given in Ref. 28 is consistent with, but much less precise than our present estimate $C^2 = 1.552(2)$. Note that the result $c \approx 0.46$ is fully consistent with $l_{\text{ex}} = 0.96(2)$ obtained in Ref. 31. Note that for our definition of the thickness one expects $c = l_{\text{ex}} - 1/2$.

Next, we fitted our data for the Ising model with the *Ansätze* (77) using $\epsilon = 0.832$. Fitting all data with $\beta \geqslant 0.202$, we get $C = 1.24653(23)$, $a = -1.3750(29)$, $c = -0.479(2)$, and $\chi^2/\text{d.o.f.} = 1.17$. Taking into account smaller values of β, $\chi^2/\text{d.o.f.}$ rapidly increases. We redid the fit using $\epsilon = 0.826$ and we also fitted with *Ansätze* that include subleading corrections. Taking into account the results of these fits, we arrive at $C = 1.247(3)$, which is fully consistent with the result (78) that we obtained from the data for the Blume-Capel model.

We performed a similar study to determine the behavior of the thermodynamic Casimir force for ++ boundary conditions for $x \to -\infty$ in the low-temperature phase. However, here we can not reach the same precision as above, since there is no efficient improved estimator for the correlation function in the low-temperature phase, and contributions due to subleading states of the transfer matix are more important than in the high-temperature phase. In the case of the Blume-Capel model- we computed $\bar{C}$ for 16 values of β in the range from $\beta = 0.39$, where $\xi = 5.584(40)$, up to $\beta = 0.405$, where $\xi = 1.5697(49)$, and in the case of the Ising model, in the range from $\beta = 0.223$, where $\xi = 6.6028(20)$, up to $\beta = 0.227$, where $\xi = 2.7321(42)$.

Analyzing the data for the Blume-Capel model, fixing $c = 0.46(2)$, we arrive at $\bar{C} = 0.428(10)$ and hence $\bar{C}^2 = 0.183(9)$, which is consistent with but more precise than $\bar{C}^2 = 0.20(5)$ given in Ref. 28. Analyzing the data for the Ising model, we get a consistent result.

C. The correction function

Plugging in $C^2(t) = C^2(1 + a_c t^\theta)$ and $\xi = \xi_0 t^{-\nu}(1 + a_\xi t^\theta)$ into Eq. (69) we get, e.g., for +− boundary conditions:

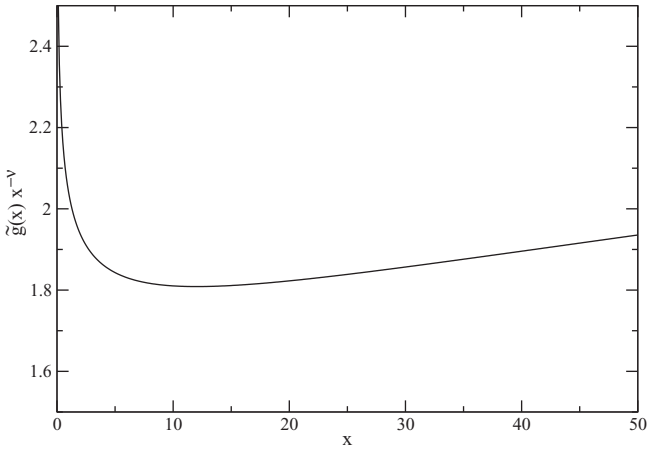

FIG. 2. We plot $\tilde{q}(x)x^{-\nu}$ as a function of the scaling variable x in the range that is relevant for our problem. For the definition of $\tilde{q}(x)$ and a discussion, see the text.

$$\begin{aligned} -\frac{\partial f_{\text{ex}}}{\partial L_0} &= L_0^{-3}C^2\frac{L_0}{\xi_0}t^\nu \exp\left(-\frac{L_0}{\xi_0}t^\nu\right) \\ &\quad\times\left\{1 + \left[a_c + \left(\frac{L_0}{\xi_0}t^\nu - 3\right)a_\xi\right]t^\theta + O(t^{2\theta})\right\} \\ &= L_0^{-3}\theta(x)\left[1 + b\tilde{q}(x)L_0^{-\omega} + \mathrm{O}\left(L_0^{-2\omega}\right)\right] \end{aligned} \tag{79}$$

with

$$b\tilde{q}(x) = \xi_0^\omega[a_c + (x^\nu - 3)a_\xi]x^\theta, \tag{80}$$

which is not consistent with

$$bq(x) = -cx^\nu \tag{81}$$

that one derives by plugging Eq. (70) into Eq. (10). In Fig. 2, we plot $\tilde{q}(x)x^{-\nu}$ as a function of x. To this end, we take the numerical values $\xi_0 = 0.1962$, $a_\xi = -0.32$, Eq. (A11), and $a_C = 2 \times 0.1962^{-0.832}(-1.375/1.247) = -8.55$. It turns out that the curve is very flat in the range of x we are interested in. Also the value is rather close to the values of c that we obtained from the analysis of data directly at the critical point.

VI. THE SCALING FUNCTION OF THE THERMODYNAMIC CASIMIR FORCE FOR ++ AND +− BOUNDARY CONDITIONS

We computed the thermodynamic Casimir force using the method discussed by Hucht.[23] Starting from the energy per area, we computed

$$\begin{aligned} &\Delta E_{\text{ex}}(L_0,\beta) \\ &\quad= [E(L_0 + d/2,\beta) - E(L_0 - d/2,\beta)]/d - E_{\text{bulk}}(\beta). \end{aligned} \tag{82}$$

The value of the energy density of the bulk system $E_{\text{bulk}}(\beta)$ is obtained from an analysis of the high-temperature series given in Ref. 41 and the low-temperature series given in Ref. 42 combined with Monte Carlo simulations. For details, see Appendix A 3.

In order to obtain $-\Delta f_{\rm ex}$, we numerically integrated $\Delta E_{\rm ex}$ using the trapezoidal rule:

$$-\Delta f_{\rm ex}(\beta_n) \approx -\Delta f_{\rm ex}(\beta_0) + \sum_{i=0}^{n-1} \frac{1}{2}(\beta_{i+1} - \beta_i) \times [\Delta E_{\rm ex}(\beta_{i+1}) + \Delta E_{\rm ex}(\beta_i)]\,, \quad (83)$$

where β_i are the values of β we simulated at. They are ordered such that $\beta_{i+1} > \beta_i$ for all i. In previous work, β_0 had been chosen such that $\Delta E_{\rm ex}(\beta_0) \approx 0$ and therefore also $-\Delta f_{\rm ex}(\beta_0) \approx 0$. Here, instead, we chose a somewhat larger value of β_0 such that the approximation discussed in the previous section is still valid. In particular, we set

$$\Delta f_{\rm ex}(\beta_0) = \pm \frac{C^2(\beta_0)}{\xi^2(\beta_0)} \frac{\exp[-(L_0+1+d/2)/\xi(\beta_0)] - \exp[-(L_0+1-d/2)/\xi(\beta_0)]}{d}, \quad (84)$$

where we have the $+$ sign for $++$ boundary conditions and the $-$ sign for $+-$ boundary conditions. By comparing results obtained with different choices of β_0, we found that the approximation (84) is accurate at the level of our statistical error up to $L_0/\xi(\beta_0) \gtrapprox 8$. To be on the safe side, we used $L_0/\xi(\beta_0) > 10$ in the following.

We simulated the Ising model with $++$ boundary conditions for the thicknesses $L_0 = 8$, 9, 14, 15, 16, 17, 18, 19, 32, 34, 64, and 68. Using the resulting data, we computed the thermodynamic Casimir force for the thicknesses $L_0 = 8.5$ and 16.5 using the difference $d = 1$. In order to check for the effect of using a finite difference to compute $\partial/\partial L_0$, we redid the calculation for $L_0 = 16.5$ using $d = 3$ and 5 in addition to 1. We conclude that $d/L_0 \approx 0.06$ is sufficient at the level of our accuracy. Therefore for $L_0 = 33$ and 66, we used $d = 2$ and 4, respectively. Throughout, we used $L > 5L_0$, which is clearly sufficient to neglect deviations from the limit $L \to \infty$; see Ref. 28. We chose $\beta_0 = 0.15$, 0.19, 0.21, and 0.218 for $L_0 = 8.5$, 16.5, 33, and 66, respectively. We simulated at 163, 122, 117, and 41 values of β for these thicknesses, respectively. Note that in the case of $L_0 = 66$, we simulated only up to β_c, since these simulation are rather expensive.

For $L_0 = 16$ and 17, we performed 6.4×10^8 measurements for each value of β that we simulated at. For each measurement, we performed 16 sweeps with the Metropolis algorithm. In total, these simulations took the equivalent of about 8 years of CPU time on one core of a Quad-Core AMD Opteron(tm) Processor 2378 running at 2.4 GHz. For $L_0 = 15$ and 18, we performed 1.3×10^8 measurements and for $L_0 = 14$ and 19, only 6.4×10^7 measurements. For $L_0 = 32$, we performed between 2.6×10^7 and 6.4×10^7 measurements and for $L_0 = 34$, we measured 2.6×10^7 or 3.2×10^7 times for each value of β. These simulations took the equivalent of about 5 years of CPU time on one core of a Quad-Core AMD Opteron(tm) Processor 2378 running at 2.4 GHz. For $L_0 = 64$ and 68, we performed 6.4×10^6 measurements for each value of β. In total, these simulations took the equivalent of about 2.5 years of CPU time on one core of a Quad-Core AMD Opteron(tm) Processor 2378 running at 2.4 GHz.

We improved the numerical results obtained in Ref. 28 for the Blume-Capel model. To this end, we simulated at additional values of β. This way both the statistical error of our result as well as the systematical error of the numerical integration are reduced. In Ref. 28, we simulated the thicknesses $L_0 = 8$, 9, 16, 17, 32, and 33. Here, we simulated $L_0 = 34$ in addition.

In Fig. 3, we plot θ_{+-}, $-\theta_{++}$ and the approximation (84) computed by using the data obtained for the Blume-Capel model at $D = 0.655$ for $L_0 = 33$ and $d = 2$. As discussed at the end of Sec. IV A, we used the value $L_s = 1.91$ to compute the effective thickness $L_{0,\rm eff} = L_0 + L_s$. The deviation of θ_{+-} and $-\theta_{++}$ from the approximation (84) is smaller than 5% for $x \gtrsim 16$ and smaller than 1% for $x \gtrsim 22.5$. The average $(\theta_{+-} - \theta_{++})/2$ deviates from the approximation (84) by less than 5% for $x \gtrsim 8.6$ and by less than 1% for $x \gtrsim 12.7$.

Next, we extracted the value and the location of the minimum of $-\Delta f_{++}$. In the case of the Blume-Capel model, we get $\beta_{\rm min} = 0.382185(15)$ and $-\Delta f_{++,\rm min} = -0.0002808(6)$ for $L_0 = 16.5$ and $\beta_{\rm min} = 0.385716(6)$ and $-\Delta f_{++,\rm min} = -0.00004117(5)$ for $L_0 = 33$. This corresponds to $t_{\rm min}(L_{0,\rm eff}/\xi_0)^{1/\nu} = 5.88(5)$ and $-L^3_{0,\rm eff}\Delta f_{++,\rm min} = -1.752(18)$ for $L_0 = 16.5$ and $t_{\rm min}(L_{0,\rm eff}/\xi_0)^{1/\nu} = 5.88(4)$ and $-L^3_{0,\rm eff}\Delta f_{++,\rm min} = -1.752(10)$ for $L_0 = 33$. The quoted error bars include the error of $\beta_{\rm min}$, $-\Delta f_{++,\rm min}$ and errors induced by the uncertainties of L_s, ξ_0, ν, and β_c. The values obtained from $L_0 = 16.5$ and 33 agree nicely. Our results are also consistent with those of Ref. 28: $x_{\rm min} = 5.82(10)$ and $\theta_{++,\rm min} = -1.76(3)$. Our results obtained for the Ising

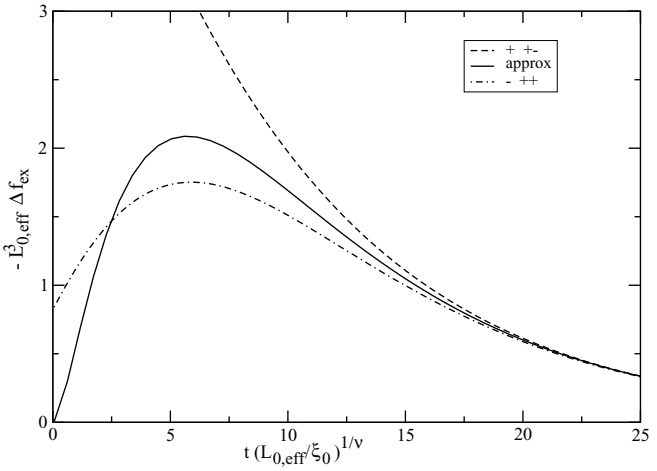

FIG. 3. We plot θ_{+-}, $-\theta_{++}$ and the approximation (84). The data are taken for the Blume-Capel model at $D = 0.655$ and the finite difference is computed from $L_0 = 32$ and 34.

TABLE IV. Results for the minimum of θ_{++} obtained for the Ising model.

$L_0 - d/2$	$L_0 + d/2$	$\beta_{\min}$	$-\Delta f_{\min}$	$L_{0,\mathrm{eff}}$	$t_{\min}(L_{0,\mathrm{eff}}/\xi_0)^{1/\nu}$
8	9	0.2123025(16)	–1.1605(1) $\times 10^{-3}$	11.471	5.96(1)
14	19	0.2176215(5)	–2.347(1) $\times 10^{-4}$		
15	18	0.2176744(19)	–2.306(1) $\times 10^{-4}$		
16	17	0.2176975(30)	–2.2869(15) $\times 10^{-4}$	19.712	5.96(1)
32	34	0.2201704(30)	–3.5996(26) $\times 10^{-5}$	36.509	5.94(2)
64	68	0.2211284(25)	–5.121(18) $\times 10^{-6}$	69.936	5.91(3)

model are summarized in Table IV. Here, we computed $L_{0,\mathrm{eff}}$ by requiring $-L_{0,\mathrm{eff}}^3 \Delta f_{\min} = -1.75169\ldots$, which is our estimate obtained for the Blume-Capel model and $L_0 = 33$. We see that the values of $L_{0,\mathrm{eff}}$ are similar to those obtained in Sec. IV from the analysis of the free energy differences at the critical point. In the last column, we give $t_{\min}(L_{0,\mathrm{eff}}/\xi_0)^{1/\nu}$ using these values of $L_{0,\mathrm{eff}}$. We see that these estimates of $x_{\min}$ are essentially consistent with that obtained above from the analysis of the Blume-Capel model.

For $L_0 = 16.5$, we checked the effect of the discretization error on the position and the value of the minimum. The error behaves as $\epsilon = ad^2 + O(d^4)$. The results obtained for $d = 1$, 3, and 5 are consistent with a quadratic behavior. For $d = 1$, the relative error is about one permille for both $-\Delta f_{\min}$ and $t_{\min}$.

In Fig. 4, we plot our numerical results for the scaling function θ_{++} that are given by $-L_{0,\mathrm{eff}}^3 \Delta f_{++}$ as a function of $t(L_{0,\mathrm{eff}}/\xi_0)^{1/\nu}$ where $\nu = 0.63002$ is set. In the case of the Blume-Capel model, we use $L_{0,\mathrm{eff}} = L_0 + 1.91$ as effective thickness of the film. We give our results for $L_0 = 16.5$ and 33.

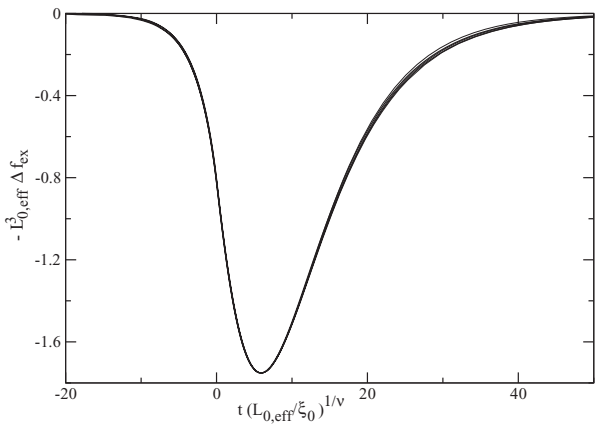

FIG. 4. We plot $-\Delta f L_{0,\mathrm{eff}}^3$ as a function of $t(L_{0,\mathrm{eff}}/\xi_0)^{1/\nu}$ for $++$ boundary conditions. The thick lines give the result obtained for the Blume-Capel model at $D = 0.655$ and the two thicknesses $L_0 = 16.5$ and 33. In the case of the Blume-Capel model, we used $L_{0,\mathrm{eff}} = L_0 + 1.91$ as the effective thickness of the film. Our results for the Ising model are given by thin lines. In the case of the Ising model, we used the effective thicknesses $L_{0,\mathrm{eff}} = 19.712$, 36.509, and 69.936 for $L_0 = 16.5$, 33, and 66, respectively. These effective thicknesses are chosen such that at the minima the curves fall on top of the one for the Blume-Capel model and $L_0 = 33$. At the resolution of the plot, all five curves fall on top of each other almost everywhere. Only for $20 \lesssim x \lesssim 40$, the curve for the Ising model and $L_0 = 16.5$ can be distinguished from the other four.

The data for $L_0 = 33$ are attached as Supplemental Material.[43] For the Ising model, we take the effective thicknesses given in the sixth column of Table IV. We plot our results for $L_0 = 16.5$, $d = 1$, $L_0 = 33$ and $L_0 = 66$. The error bars are too small to be visible in the plot. At the resolution of the plot, all five curves fall on top of each other almost everywhere. Only for $20 \lesssim x \lesssim 40$, the curve for the Ising model and $L_0 = 16.5$ can be distinguished from the other four.

Next, we discuss our numerical results for the scaling function θ_{+-}. In Fig. 5, we plot $-\Delta f L_{0,\mathrm{eff}}^3$ as a function of $t(L_{0,\mathrm{eff}}/\xi_0)^{1/\nu}$ for the Blume-Capel model at the thicknesses $L_0 = 16.5$ and 33 and the Ising model at $L_0 = 16.5$, 33, and 66. In the case of the Blume-Capel model, we use $L_{0,\mathrm{eff}} = L_0 + L_s$ with $L_s = 1.91$. For the Ising model, we take the same values for $L_{0,\mathrm{eff}}$ as above for $++$ boundary conditions.

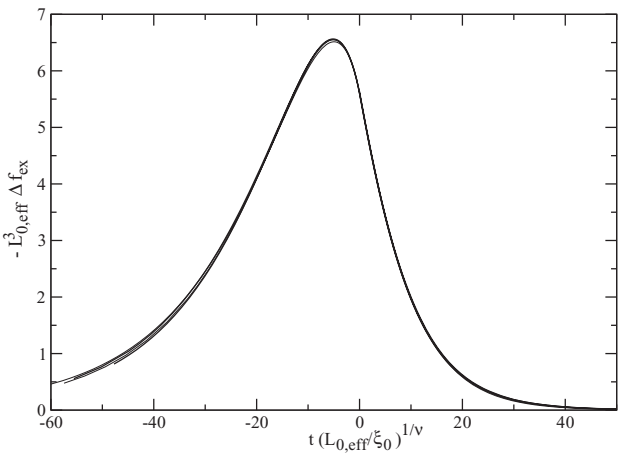

FIG. 5. We plot $-\Delta f L_{0,\mathrm{eff}}^3$ as a function of $t[L_{0,\mathrm{eff}}/\xi_0]^{1/\nu}$ for $+-$ boundary conditions. The thick lines give the result obtained for the Blume-Capel model at $D = 0.655$ and the two thicknesses $L_0 = 16.5$ and 33. In the case of the Blume-Capel model, we used $L_{0,\mathrm{eff}} = L_0 + 1.91$ as the effective thickness of the film. The data for $L_0 = 33$ are attached as Supplemental Material.[43] Our results for the Ising model are given by thin lines. In the case of the Ising model, we used the effective thicknesses $L_{0,\mathrm{eff}} = 19.712$, 36.509, and 69.936, for $L_0 = 16.5$, 33, and 66, respectively. These values are taken from the analysis of $++$ boundary conditions above. At the resolution of the plot, all five curves fall on top of each other almost everywhere. Near the maximum, the curve for the Ising model and $L_0 = 16.5$ stays slightly below the other ones. For $x \lesssim -30$ the curves slightly fork. Note that in this range, the difference between the Blume-Capel results for $L_0 = 16.5$ and 33 is of a similar size as the one between the Ising results for $L_0 = 16.5$ and 33 and between Blume-Capel and Ising models.

TABLE V. Results for the maximum of θ_{+-} obtained for Blume Capel (BC) model and the Ising (I) model. In the second and third columns, we give the thicknesses that have been considered. In the fourth column, we give the value of $-\Delta f$ at the maximum and in the fifth column, we give the location of the maximum. In the sixth and seventh columns, we give estimates of $\theta_{+-,\max}$ and $x_{\max}$ derived from these results.

Model	$L_0 - d/2$	$L_0 + d/2$	$\beta_{\max}$	$-\Delta f_{\max}$	$-L_{0,\mathrm{eff}}^3 \Delta f_{\max}$	$t_{\max}(L_{0,\mathrm{eff}}/\xi_0)^{1/\nu}$
BC	16	17	0.39257(3)	0.0010501(7)	6.552(5)[54]	–5.15(3)[3]
BC	32	34	0.389474(5)	0.00015426(5)	6.563(2)[28]	–5.139(15)[15]
I	16	17	0.224948(4)	0.00085044(30)	6.514(2)	–4.959(6)
I	32	34	0.2229119(3)	0.000134650(35)	6.552(2)	–5.035(12)

We find that the different curves fall quite nicely on top of each other. In the neighbourhood of the maximum, the curve for the Ising model at $L_0 = 16.5$ lies slightly below the other ones and for $x \lesssim -30$ the curves slightly fork. The discrepancies discussed for $++$ boundary conditions in the range $20 \lesssim x \lesssim 40$ are also present for $+-$ boundary conditions. They can not be seen in Fig. 5 since the range of values for $+-$ boundary conditions is larger than that for $++$ boundary conditions.

In Table V, we summarize results for the maximum of θ_{+-}. Using $L_s = 1.91$ in the case of the Blume-Capel model, we get nicely consistent results for $x_{\max}$ and $\theta_{+-,\max}$ from the two thicknesses $L_0 = 16.5$ and 33. These results improve those of Ref. 28: $x_{+-,\max} = -5.17(7)$ and $\theta_{+-,\max} = 6.56(10)$. In the case of the Ising model, we use the values of $L_{0,\mathrm{eff}}$ obtained above for films with $++$ boundary conditions. The resulting estimates for $x_{\max}$ and $\theta_{+-,\max}$ are close to those obtained from the Blume-Capel model. In particular, the results obtained for $L_0 = 33$ are closer to the Blume-Capel ones than those obtained for $L_0 = 16.5$.

We conclude that our numerical results for the scaling functions of the thermodynamic Casimir force for $++$ and $+-$ boundary conditions are fully consistent with the universality hypothesis. Furthermore, our *Ansätze* (8) provides a good approximation of the universal correction function.

VII. SUMMARY AND CONCLUSIONS

We studied the spin-1/2 Ising model and the improved Blume-Capel model on the simple cubic lattice with film geometry. In particular, we considered strongly symmetry breaking $++$ and $+-$ boundary conditions. We focused on the thermodynamic Casimir force. At the critical point, we studied the behavior of the free energy per area, the energy per area, the magnetization profile, and the second-moment correlation length of the film. The main subject of the present work is about corrections to scaling. Previously, it has been demonstrated at the example of improved models that corrections $\propto L_0^{-1}$ that are due to the boundaries can be expressed by an effective thickness $L_{0,\mathrm{eff}} = L_0 + L_s$, where L_s is the same for all quantities. Note that L_s depends on the model and, in particular, on the details of the boundary conditions. Here, we probed the hypothesis that the leading bulk corrections can be expressed in an analogous way:

$$L_{0,\mathrm{eff}} = L_0 + L_s + c(L_0 + L_s)^{1-\omega}. \tag{85}$$

Fitting various quantities at the critical point of the Ising model we find similar, but likely not identical values of the amplitude c. Also the study of the thermodynamic Casimir force for large values of the scaling variable x shows that Eq. (85) can not be exact. Nevertheless, it turns out to be a surprisingly good approximation in the range of x that is of experimental interest. In Sec. VI, we investigate the thermodynamic Casimir force for $++$ and $+-$ boundary conditions. We find for $-\Delta f L_{0,\mathrm{eff}}^3$ plotted as a function of $t(L_{0,\mathrm{eff}}/\xi_0)^{1/\nu}$, a good collapse of the data for both the spin-1/2 Ising and the Blume-Capel models. In the case of the Blume-Capel model, we used $L_{0,\mathrm{eff}} = L_0 + L_s$ with $L_s = 1.91(5)$. We demonstrated that in the case of the spin-1/2 Ising model approximately the same $L_{0,\mathrm{eff}}$ can be used for $++$ and $+-$ boundary conditions. The values of $L_{0,\mathrm{eff}}$ that we obtained in Sec. VI for $L_0 = 16.5$, 33, and 66 are similar to those obtained from the analysis of $D_{f,+-,++}$ in Sec. IV A. The estimates of L_s and c obtained from this analysis are highly anticorrelated. From the analysis of $D_{f,+-,++}$, we get $L_s = 0.9$ and $c = 1.5$ as central estimates. The range of possible values is given by $L_s = 1.1$, $c = 1.4$ one side and $L_s = 0.8$, $c = 1.6$ at the other. Note that the value of L_s depends on the definition of the thickness. In particular, when comparing with the Refs. 24, 25, and 30 by Vasilyev, Gambassi, Maciołek, and Dietrich (VGMD) one should take into account that $L_{0,\mathrm{VGMD}} = L_{0,\mathrm{ours}} + 2$ and hence $L_{s,\mathrm{VGMD}} = L_{s,\mathrm{ours}} - 2$. Since the correction function $q(x)$ is universal, also for experimental data or data obtained from the numerical study of other models, an effective thickness (85) should parametrize leading corrections quite well. Note again that L_s should depend on the microscopic details of the system. In the case of the amplitude c, universal ratios can be constructed. For example,

$$\frac{c}{a_{\xi,+}\xi_0^{\omega}} = -8(2), \tag{86}$$

where we used the numerical values of $a_{\xi,+}$ and ξ_0 obtained in Appendix. In Introduction, we argued that Eq. (8) provides a good approximation for the corrections to scaling function since fluctuations are strongly suppressed near the boundaries of the film. Therefore Eq. (8) should not work for periodic and antiperiodic boundary conditions. Furthermore, the amplitude of leading corrections should be smaller in these cases, which is indeed confirmed by the numerical results[44] for periodic boundary conditions.

Furthermore, we improved the numerical accuracy of the estimates of the universal scaling functions θ_{++} and θ_{+-}. Writing the partition function in terms of eigenvalues and eigenstates of the transfer matrix and boundary states, one finds for large values of x,

$$\theta_{++}(x) = -\theta_{+-}(x) = -C^2 x^{3\nu} \exp(-x^{\nu}). \tag{87}$$

Here, we demonstrated how C^2 can be accurately computed by analyzing the magnetization profile of films and the bulk correlation function. We find

$$C^2 = 1.552(2). \tag{88}$$

This result can be compared with $C^2 = 1.5(1)$ obtained in Ref. 28.

At the critical point, we find by studying the difference of free energies per area,

$$\Delta_{+-} - \Delta_{++} = [\theta_{+-}(0) - \theta_{++}(0)]/2 = 3.204(5), \tag{89}$$

where we average the results obtained from the analysis of the spin-1/2 Ising and the improved Blume-Capel model. For the slope of the scaling function at the critical point, we find

$$\theta'_{+-}(0) = -0.482(2), \quad \theta'_{++}(0) = -0.318(2). \tag{90}$$

The minimum of θ_{++} is located at $x_{\min} = 5.88(4)$ and takes the value $\theta_{++,\min} = -1.752(10)$. For the maximum of θ_{+-}, we get $x_{\max} = -5.14(3)$ and $\theta_{+-,\max} = 6.56(3)$. The reduction of the error compared with Ref. 28 is mainly due to the fact that here we assume $L_s = 1.91(5)$ instead of $L_s = 1.9(1)$ as in Ref. 28.

ACKNOWLEDGMENT

This work was supported by the DFG under the grant No. HA 3150/2-2.

APPENDIX: NUMERICAL RESULTS FOR THE SPIN-1/2 ISING BULK SYSTEM

1. The critical point

We extended the study of Ref. 7 by simulating the Ising model on the simple cubic lattice on a system of the size L^3 with $L = 400$ and periodic boundary conditions in all three directions at $\beta = 0.2216546$. As in Ref. 7, we simulated the model by using a hybrid of the local Metropolis, the single cluster,[36] and the wall cluster algorithms.[45] For details, see Sec. IV of Ref. 7. We performed 2.3×10^7 measurements. In total, this simulation took the equivalent of about four years of CPU time on a single core of a Quad-Core AMD Opteron(tm) Processor 2378 running at 2.4 GHz. In the first step of the analysis, we determined β_c by analyzing the behavior of the renormalization group invariant quantities Z_a/Z_p, $\xi_{2\mathrm{nd}}/L$, U_4, and U_6. For the definition of these quantities see Sec. II of Ref. 7. We fitted our data for the Ising model with the *Ansätze*

$$R(\beta_c, L) = R^* + aL^{-\omega} + bL^{-2}, \tag{A1}$$

where R denotes one of the renormalization group invariant quantities. Performing these fits, we used the results for R^* given in Table V of Ref. 7 as input. Furthermore, we fixed $\omega = 0.832$. We get acceptable χ^2/d.o.f. for fits with $L_{\min} \geqslant 16$. The statistical error of β_c increases only slowly with increasing $L_{\min}$. Based on fits with $L_{\min} \geqslant 24$ for Z_a/Z_p and $\xi_{2\mathrm{nd}}/L$, we arrive at $\beta_c = 0.22165462(2)$. Instead, analyzing U_4 and U_6, we arrive at $\beta_c = 0.22165463(2)$. In Ref. 46, the authors computed the Binder cumulant U_4 on lattices of a linear size up to $L = 1536$. Fitting their data, taking the value $U_4^* = 1.6036(1)$[7] as input, we arrive at $\beta_c = 0.221654615(10)$. In this work, we shall use

$$\beta_c = 0.22165462(2). \tag{A2}$$

This estimate can be compared, e.g., with the previous estimates $\beta_c = 0.22165463(8)$ obtained in Ref. 7 using a linear lattice size up to $L = 96$ and $\beta_c = 0.22165455(3)$ given in Table X in Ref. 47.

At the critical point, the energy density behaves as

$$E_{\mathrm{bulk}}(L) = E_{ns} + aL^{3-1/\nu}(1 + bL^{-\omega} + \dots). \tag{A3}$$

Performing various fits based on Eq. (A3), using the data of Ref. 7, and our result for $L = 400$, we arrive at

$$E_{ns} = 0.9906065(15) + 85(\beta_c - 0.22165462). \tag{A4}$$

The specific heat behaves as

$$C_{\mathrm{bulk}}(L) = C_{ns} + aL^{3-2/\nu}(1 + bL^{-\omega} + \dots) \tag{A5}$$

performing various fits based on Eq. (A3), using the data of Ref. 7, and our result for $L = 400$, we arrive at

$$C_{ns} = -29.1(3) - 7\,700\,000(\beta_c - 0.22165462) - 3300(\nu - 0.63002). \tag{A6}$$

2. Amplitudes and amplitude ratios

We simulated the three-dimensional Ising model for a large number of β values in the high- and the low-temperature phase on L^3 lattices with periodic boundary conditions in all three directions. We have chosen the linear lattice size such that $L > 10\xi_{2\mathrm{nd}}(\beta)$ in order to keep deviations from the thermodynamic limit sufficiently small to be ignored in the analysis of the data. For the precise definition of the observables, see Sec. II in Ref. 33. In the high-temperature phase, we simulated at 68 values of β in the range $0.125 \leqslant \beta \leqslant 0.2213$. To give the reader an impression of the quality of the data, we give the results for the five largest values of β in Table VI. Analogous results for the low-temperature phase are given in Table VII.

First, we fitted our data for the second-moment correlation length in the high-temperature phase using the *Ansätze*

$$\xi_{2\mathrm{nd}} = \xi_{2nd,0,+} t^{-\nu}(1 + a_{\xi,+} t^{\theta}), \tag{A7}$$

$$\xi_{2\mathrm{nd}} = \xi_{2nd,0,+} t^{-\nu}(1 + a_{\xi,+} t^{\theta} + bt), \tag{A8}$$

and

$$\xi_{2\mathrm{nd}} = \xi_{2nd,0,+} t^{-\nu}(1 + a_{\xi,+} t^{\theta} + bt + ct^{2\nu}), \tag{A9}$$

TABLE VI. The second moment correlation length $\xi_{2\mathrm{nd}}$, the magnetic susceptibility χ, and the energy density E_{bulk} for the five largest values of the inverse temperature β that we simulated in the high-temperature phase of the Ising model. We simulated L^3 systems with periodic boundary conditions in all three directions.

β	L	$\xi_{2\mathrm{nd}}$	χ	E_{bulk}
0.2206	200	14.57699(31)	831.162(32)	0.96369936(90)
0.2207	200	15.5321(10)	940.79(11)	0.9656874(29)
0.2208	200	16.6644(11)	1079.27(14)	0.9677195(31)
0.2210	300	19.73548(63)	1501.960(86)	0.97198710(87)
0.2213	400	29.1058(11)	3212.44(23)	0.97909806(69)

TABLE VII. The second moment correlation length ξ_{2nd}, the magnetic susceptibility χ, the magnetisation m, and the energy density E_{bulk} for the five smallest values of the inverse temperature β that we simulated in the low-temperature phase of the Ising model. We simulated L^3 systems with periodic boundary conditions in all three directions.

β	L	ξ_{2nd}	χ	m	E_{bulk}
0.2219	300	18.930(40)	1058.49(66)	0.1815607(39)	1.0126483(10)
0.2220	200	15.294(24)	690.78(38)	0.2027298(54)	1.0200656(17)
0.2221	200	12.976(28)	501.95(30)	0.2200006(48)	1.0271260(16)
0.2222	170	11.418(17)	389.43(17)	0.2347800(43)	1.0339257(16)
0.2223	170	10.278(13)	315.26(12)	0.2477779(38)	1.0405068(16)

where $t = \beta_c - \beta$. We fixed $\beta_c = 0.22165462$, $\nu = 0.63002$, and $\omega = 0.832$. Based on a large number of fits using these *Ansätze*, we conclude

$$\xi_{2nd,0,+} = 0.1962(1) + 540(\beta_c - 0.22165462) - 1.8(\nu - 0.63002) - 0.002(\omega - 0.832) \quad \text{(A10)}$$

and

$$a_{\xi,+} = -0.32(3) - 120000(\beta_c - 0.22165462) + 130(\nu - 0.63002) - 1.1(\omega - 0.832). \quad \text{(A11)}$$

Our result is in nice agreement with that of Ref. 48 obtained by analyzing the high-temperature series of ξ_{2nd}. In Table VII in Ref. 48, the authors quote $\xi_{0,+} = 0.5070(5)$ for the definition $\tilde{t} = (\beta_c - \beta)/\beta_c$ of the reduced temperature. Converting to our convention one gets $\xi_{0,+} = 0.5070(5) \times 0.22165462^{0.63002} = 0.1962(2)$.

In a similar way, we analyzed the second-moment correlation length in the low-temperature phase and the magnetic susceptibility in both phases. Let us summarize the final results:

$$\xi_{2nd,0,-} = 0.1015(2) - 200(\beta_c - 0.22165462) - 0.9(\nu - 0.63002) - 0.001(\omega - 0.832) \quad \text{(A12)}$$

and

$$a_{\xi,-} = -0.55(15) + 70000(\beta_c - 0.22165462) + 100(\nu - 0.63002) - 2.2(\omega - 0.832). \quad \text{(A13)}$$

Using the results (A10) and (A12), we get for the universal ratio $\xi_{2nd,0,+}/\xi_{2nd,0,-} = 1.933(5)$, which is fully consistent with $\xi_{2nd,0,+}/\xi_{2nd,0,-} = 1.939(5)$ obtained in Ref. 33 by analyzing Monte Carlo data obtained for the Blume-Capel model at $D = 0.655$.

Analyzing the data for the magnetic susceptibility in the high-temperature phase, we arrive at

$$C_+ = 0.1739(1) + 800(\beta_c - 0.22165462) - 1.6(\gamma - 1.2372) - 0.0013(\omega - 0.832) \quad \text{(A14)}$$

and

$$a_{\chi,+} = -0.33(5) - 150\,000(\beta_c - 0.22165462) + 100(\gamma - 1.2372) - 1.3(\omega - 0.832). \quad \text{(A15)}$$

The corresponding results for the low-temperature phase are

$$C_- = 0.03695(2) - 200(\beta_c - 0.22165462) - 0.35(\gamma - 1.2372) - 0.001(\omega - 0.832) \quad \text{(A16)}$$

and

$$a_{\chi,-} = -1.6(2) + 20\,000(\beta_c - 0.22165462) + 120(\gamma - 1.2372) - 7(\omega - 0.832). \quad \text{(A17)}$$

The ratio $C_+/C_- = 4.706(8)$ is consistent with $C_+/C_- = 4.713(7)$ obtained in Ref. 33 by analyzing Monte Carlo data obtained for the Blume-Capel model at $D = 0.655$. Note that our estimates are slightly smaller than $C_+/C_- = 4.78(3)$ obtained from series expansions.[48]

3. The energy density

In order to compute the thermodynamic Casimir force, we need the energy density of the bulk system for a large number of β values. To this end, the authors of Ref. 44 used the results of Ref. 49 in combination with a naive evaluation of the high-[41] and low-temperature[50] series. Here, instead, we combined the analysis of the high-[41] and low-temperature[42] series with the results of our Monte Carlo simulations discussed above. The analysis of the high-temperature series is simpler and the results are more accurate than that of the low-temperature one. This is due to the fact that the high-temperature series converges up to the critical point, while this is not the case for the low-temperature series.

In the neighbourhood of the critical point, the energy density behaves as

$$E_{bulk} = E_{ns} - C_{ns}t + \cdots + a_\pm |t|^{1-\alpha} \times (1 + b_\pm |t|^\theta + \dots) + \dots. \quad \text{(A18)}$$

We analyzed both series using differential approximants. In particular, we used the second-order differential equation given in Eq. (6.16) of Ref. 51:

$$u^2 Q_2(u) g''(u) + u Q_1(u) g'(u) + Q_0(u) g(u) = R(u), \quad \text{(A19)}$$

where $Q_2(u)$, $Q_1(u)$, $Q_0(u)$, and $R(u)$ are polynomials in the expansion variable u of the order J, K, L, and M, respectively. These polynomials are fixed by the requirement that the function $g(u)$ has the correct expansion in u up to the highest known order. The differential Eq. (A19) is used, since it is known that its solution behaves as

$$g(u) = g_{ns}(u) + a_1(u)(u_c - u)^{-x_1} + a_2(u)(u_c - u)^{-x_2}, \quad \text{(A20)}$$

where $g_{ns}(u)$, $a_1(u)$ and $a_2(u)$ are analytic functions.

Usually one sets $Q_2(0) = 1$. Therefore $J + K + L + M = N - 2$, where N is the order of the last known coefficient of the series. We biased the analysis by using our estimate (A2)

of the inverse critical temperature and our estimates of ν and ω.[7] This way, additional coefficients of the polynomials are fixed and one gets $J + K + L + M = N + 3$. For a detailed discussion, we refer the reader to Sec. 6 of Ref. 51. We solved the differential equation (A19) numerically by using the Runge-Kutta method.

In the high-temperature phase, Arisue and Fujiwara[41] computed the free energy density of the bulk system as a series in $v = \tanh(\beta)$ up to $O(v^{46})$. Note that the coefficients of odd orders vanish and hence the free energy density can be expressed as a series in $u = v^2 = \tanh^2(\beta)$. Since we are aiming at the energy density, we actually analyzed

$$\tilde{E} = -\frac{\partial f}{\partial u}. \tag{A21}$$

The energy density is then given by

$$E_{\rm bulk} = -\frac{\partial f}{\partial \beta} = -\frac{\partial f}{\partial u}\frac{\partial u}{\partial \beta} = 2\tanh(\beta)[1-\tanh^2(\beta)]\ \tilde{E}. \tag{A22}$$

The free energy density is given by

$$-f(\beta) = \ln 2 + 3\ln[\cosh(\beta)] + \sum_{i=0}^{46} a_i v^i + O(v^{48}), \tag{A23}$$

where the coefficients a_i are given in Table I of the preprint version of Ref. 41.

We computed $\chi^2 = \sum_i \{[E_{\rm series}(\beta_i) - E_{\rm MC}(\beta_i)]/e(\beta_i)\}^2$, where $E_{\rm series}(\beta_i)$ and $E_{\rm MC}(\beta_i)$ are the estimates obtained from the analysis of the series and from the Monte Carlo simulations, respectively, and $e(\beta_i)$ is the statistical error of the Monte Carlo result at the inverse temperature β_i. We find that a large fraction of the possible choices of J, K, L, and M result in a χ^2/d.o.f. ≈ 1.03. About 91% of the possible choices have χ^2/d.o.f. < 1.073 and about 92.5% have χ^2/d.o.f. < 1.305.

We computed numerically E_{ns}, C_{ns}, a_+, and a_+b_+ as defined by Eq. (A18). Averaging over all choices of J, K, L, and M with χ^2/d.o.f. < 1.073, we get

$$E_{ns} = 0.9906058(8) + 32(\beta_c - 0.22165462) - 0.0069(\nu - 0.63002) + 0.0000072(\omega - 0.832), \tag{A24}$$

$$C_{ns} = -29.07(3) - 234\,000(\beta_c - 0.22165462) - 1960(\nu - 0.63002) - 0.86(\omega - 0.832), \tag{A25}$$

$$a_+ = -25.715(12) - 92\,500(\beta_c - 0.22165462) - 1390(\nu - 0.63002) - 0.244(\omega - 0.832), \tag{A26}$$

and

$$a_+b_+ = 3.87(28) - 1\,300\,000(\beta_c - 0.22165462) - 2900(\nu - 0.63002) + 13(\omega - 0.832). \tag{A27}$$

The number given in parentheses is the variance over all choices of J, K, L, and M with χ^2/d.o.f. < 1.073. It might serve as a lower bound of the systematic error of the analysis of the series. Since the estimates for E_{ns} and C_{ns} obtained here are in good agreement with those obtained from the finite size analysis of Monte Carlo data given above, we are confident that also in the case of a_+ and a_+b_+ the variance over the choices of J, K, L, and M is a realistic estimate of the systematical error. Analyzing the series for the free energy density itself, we get

$$-f_{ns} = \ln 2 + 0.0847028611(4) + 0.99(\beta_c - 0.22165462) + 0.000001(\nu - 0.63002). \tag{A28}$$

The estimate of f_{ns} strongly depends on the input value for β_c. The dependence on ν is small and that on ω can be ignored.

In order to calculate the energy density that is needed as input to compute the thermodynamic Casimir force, we picked, to some extend *ad hoc*, the approximant characterized by $J = 7$, $K = 7$, $L = 5$, and $M = 6$, which is characterized by the fact that the order of all four polynomials is similar, χ^2/d.o.f $= 1.029$ and $E_{ns} = 0.9906063$ for $\beta_c = 0.22165462$, $\nu = 0.63002$, and $\omega = 0.832$ fixed. Comparing with other acceptable choices for J, K, L, and M, we find that, e.g., for $\beta = 0.2216$, the differences are of the order 10^{-7} and for $\beta = 0.22$ of the order 10^{-8}. Compared with the statistical error of $[E(L_0 + d/2,\beta) - E(L_0 - d/2,\beta)]/d$, see Eq. (82), errors of this size are negligible.

In the low-temperature phase, Vohwinkel[42] computed the energy density as a series in $u = \exp(-4\beta)$ up to $O(u^{32})$. Unfortunately, in this case, there is no choice of J, K, L, and M that allows to fit our Monte Carlo data down to $\beta = 0.2219$. The best that we could find are the two choices $J = 9$, $K = 6$, $L = 7$, and $M = 13$ and $J = 20$, $K = 6$, $L = 3$, and $M = 6$ that fit our Monte Carlo data with an acceptable χ^2/d.o.f. for $\beta \geqslant 0.228$ and $\beta \geqslant 0.231$, respectively. The linear combination $0.8155E_{9,6,7,13} + 0.1845E_{20,6,3,6}$ fits all of our data in the low-temperature phase with χ^2/d.o.f. $= 1.25$.

Since this result is not fully satisfying, we fitted our data with various *Ansätze* based on Eq. (A18). In particular, the *Ansatz*

$$E = E_{ns} - C_{ns}t + d_{ns}t^2 + a_-(-t)^{1-\alpha} + a_-b_-(-t)^{1-\alpha+\theta} + b(-t)^{2-\alpha} + c(-t)^{2-\alpha-\theta} \tag{A29}$$

fits our data up to $\beta = 0.246$ with χ^2/d.o.f. $= 1.15$, where we fixed $E_{ns} = 0.9906065$, $C_{ns} = -29.07$, $\alpha = 0.10994$, and $\omega = 0.832$. Fitting all 55 data points up to $\beta = 0.241$, we get for the free parameters $a_- = 47.9436$, $a_-b_- = -16.336$, $b = -363.5$, $d_{ns} = 269.2$, and $c = 287.3$. In order to calculate the bulk energy that is needed for the computation of the thermodynamic Casimir force, we used for $\beta \geqslant 0.228$ the linear combination $0.8155E_{9,6,7,13} + 0.1845E_{20,6,3,6}$ of approximants and for $0.228 > \beta \geqslant \beta_c$, we used Eq. (A29) together with the results for the free parameters quoted above. For a quite large range of β, the two approaches to represent the bulk energy give consistent results. For $0.2219 \leqslant \beta \leqslant 0.2394$, the difference between the two is less than 3×10^{-6}. The deviation of our result from that of Ref. 49 is typically of the order 10^{-5}.

Taking into account various fits and, in particular, computing the dependence of the result on the values of the input

parameters, we arrive at

$$a_- = 47.96(1) + 2\,350\,000(\beta_c - 0.22165462) + 2500(\nu - 0.63002) - 0.16(\omega - 0.832) - 0.44(C_{ns} - 29.1) - 3700(E_{ns} - 0.9906065), \quad \text{(A30)}$$

and hence

$$\frac{A_+}{A_-} = -\frac{a_+}{a_-} = 0.5362(20), \quad \text{(A31)}$$

which is fully consistent with the estimate $A_+/A_- = 0.536(2)$ obtained by studying the Blume-Capel model at $D = 0.655$.[33] Note that the error of our estimate of A_+/A_- is dominated by the uncertainty of C_{ns} that we use as input for our fits in the low-temperature phase. Here, we took the error of the estimate obtained from the finite size scaling analysis at the critical point, Eq. (A6). The systematic error of the estimate obtained from the analysis of the high-temperature series is likely smaller, but difficult to estimate. The authors of Ref. 48 quote $A_+/A_- = 0.530(3)$, which is slightly smaller than our results. For a summary of estimates presented in the literature, see Table IV or Ref. 48.

*Martin.Hasenbusch@physik.hu-berlin.de

[1] K. G. Wilson and J. Kogut, Phys. Rep. C **12**, 75 (1974).
[2] M. E. Fisher, Rev. Mod. Phys. **46**, 597 (1974).
[3] M. E. Fisher, Rev. Mod. Phys. **70**, 653 (1998).
[4] A. Pelissetto and E. Vicari, Phys. Rep. **368**, 549 (2002).
[5] F. J. Wegner, J. Math. Phys. **10**, 2259 (1971).
[6] F. J. Wegner, in *Phase Transitions and Critical Phenomena*, edited by C. Domb and M. S. Green (Academic Press, New York, 1976), Vol. 6.
[7] M. Hasenbusch, Phys. Rev. B **82**, 174433 (2010).
[8] K. E. Newman and E. K. Riedel, Phys. Rev. B **30**, 6615 (1984).
[9] M. Campostrini, A. Pelissetto, P. Rossi and E. Vicari, Phys. Rev. E **57**, 184 (1998).
[10] M. N. Barber, *Finite-size Scaling* in Phase Transitions and Critical Phenomena Vol. 8, edited C. Domb and J. L. Lebowitz, (Academic Press, 1983).
[11] K. Binder, *Critical Behaviour at Surfaces* in Phase Transitions and Critical Phenomena Vol. 8, edited C. Domb and J. L. Lebowitz, (Academic Press, 1983).
[12] H. W. Diehl, *Field-theoretical Approach to Critical Behaviour at Surfaces* in Phase Transitions and Critical Phenomena Vol. 10, edited by C. Domb and J. L. Lebowitz (Academic, London 1986), p. 76.
[13] H. W. Diehl, Int. J. Mod. Phys. B **11**, 3503 (1997).
[14] M. E. Fisher and P.-G. de Gennes, C. R. Acad. Sci., Ser. B **287**, 207 (1978).
[15] M. Krech, *The Casimir Effect in Critical Systems* (World Scientific, Singapore, 1994).
[16] Daniel Dantchev, Michael Krech, and S. Dietrich, Phys. Rev. E **67**, 066120 (2003).
[17] Daniel Dantchev, Frank Schlesener, and S. Dietrich, Phys. Rev. E **76**, 011121 (2007).
[18] R. Garcia and M. H. W. Chan, Phys. Rev. Lett. **83**, 1187 (1999).
[19] A. Ganshin, S. Scheidemantel, R. Garcia, and M. H. W. Chan, Phys. Rev. Lett. **97**, 075301 (2006).
[20] M. Fukuto, Y. F. Yano, and P. S. Pershan, Phys. Rev. Lett. **94**, 135702 (2005).
[21] C. Hertlein, L. Helden, A. Gambassi, S. Dietrich, and C. Bechinger, Nature (London) **451**, 172 (2008).
[22] A. Gambassi, A. Macioł ek, C. Hertlein, U. Nellen, L. Helden, C. Bechinger, and S. Dietrich, Phys. Rev. E **80**, 061143 (2009).
[23] A. Hucht, Phys. Rev. Lett. **99**, 185301 (2007).
[24] O. Vasilyev, A. Gambassi, A. Maciołek, and S. Dietrich, Phys. Rev. E **79**, 041142 (2009).
[25] O. Vasilyev, A. Gambassi, A. Maciołek, and S. Dietrich, Europhys. Lett. **80**, 60009 (2007).
[26] A. Gambassi, J. Phys. Conf. Series **161**, 012037 (2009).
[27] M. Hasenbusch, J. Stat. Mech. (2009) P07031.
[28] M. Hasenbusch, Phys. Rev. B **82**, 104425 (2010).
[29] M. Campostrini, M. Hasenbusch, A. Pelissetto, and E. Vicari, Phys. Rev. B **74**, 144506 (2006).
[30] O. Vasilyev, A. Maciołek, and S. Dietrich, Phys. Rev. E **84**, 041605 (2011).
[31] M. Hasenbusch, Phys. Rev. B **83**, 134425 (2011).
[32] Y. Deng and H. W. J. Blöte, Phys. Rev. E **70**, 046111 (2004).
[33] M. Hasenbusch, Phys. Rev. B **82**, 174434 (2010).
[34] M. Campostrini, A. Pelissetto, P. Rossi, and E. Vicari, Phys. Rev. E **65**, 066127 (2002).
[35] M. Hasenbusch and K. Pinn, Physica A **203**, 189 (1994).
[36] U. Wolff, Phys. Rev. Lett. **62**, 361 (1989).
[37] R. C. Brower and P. Tamayo, Phys. Rev. Lett. **62**, 1087 (1989).
[38] M. Saito and M. Matsumoto, *SIMD-oriented Fast Mersenne Twister: a 128-bit Pseudorandom Number Generator* in Monte Carlo and Quasi-Monte Carlo Methods 2006, edited by A. Keller, S. Heinrich, and H. Niederreiter (Springer, 2008); M. Saito, Masters thesis, Hiroshima University, 2007. The source code of the program is provided at [http://www.math.sci.hiroshima-u.ac.jp/~m-mat/MT/SFMT/index.html].
[39] M. Hasenbusch, J. Phys. I (France) **3**, 753 (1993).
[40] M. Hasenbusch, Physica A **197**, 423 (1993).
[41] H. Arisue and T. Fujiwara, Phys. Rev. E **67**, 066109 (2003), there is a typo in the 42th order term, the correct value appears in e-print arXiv:hep-lat/0209002.
[42] C. Vohwinkel, Phys. Lett. B **301**, 208 (1993); and private communication.
[43] See Supplemental Material at http://link.aps.org/supplemental/10.1103/PhysRevB.85.174421 for numerical results for θ_{++} and θ_{+-}.
[44] Alfred Hucht, Daniel Grüneberg, and Felix M. Schmidt, Phys. Rev. E **83**, 051101 (2011).
[45] M. Hasenbusch, K. Pinn, and S. Vinti, Phys. Rev. B **59**, 11471 (1999).
[46] J. Kaupužs, J. Rimšāns, and R. V. N. Melnik, Ukr. J. Phys. **56**, 845 (2011).

[47] Y. Deng and H. W. J. Blöte, Phys. Rev. E **68**, 036125 (2003).
[48] P. Butera and M. Pernici, Phys. Rev. B **83**, 054433 (2011).
[49] X. Feng and H. W. J. Blöte, Phys. Rev. E **81**, 031103 (2010).
[50] G. Bhanot, M. Creutz, I. Horvath, J. Lacki, and J. Weckel, Phys. Rev. E **49**, 2445 (1994).
[51] A. J. Guttmann, *Asymptotic Analysis of Power-Series Expansions* in Phase Transitions and Critical Phenomena Vol. 13, edited by C. Domb and J. L. Lebowitz (Academic, London 1989), p. 71.